North Atlantic Holocene climate evolution recorded by high-resolution terrestrial and marine biomarker records

Moossen, Heiko; Bendle, James; Seki, Osamu; Quillmann, Ursula; Kawamura, Kimitaka

DOI:
10.1016/j.quascirev.2015.10.013

North Atlantic Holocene climate evolution recorded by high-resolution terrestrial and marine biomarker records.

Heiko Moossen[1*], James Bendle[1], Osamu Seki[2], Ursula Quillmann[3], Kimitaka Kawamura[2],

[1] School of Geographical, Earth and Environmental Sciences; University of Birmingham; B15 2TT Birmingham; UK

[2] Institute of Low Temperature Science, Hokkaido University, N19W8, Kita-ku, 8 Sapporo, Hokkaido, 060-0819, Japan

[3] Institute of Arctic and Alpine Research, University of Colorado, 1560 30th Street, Boulder, CO 80309, USA

Key Words: Iceland, GDGT, alkenone; *n*-alkane; Holocene; climate reconstruction

Please cite as:

Moossen, H., Bendle, J., Seki, O., Quillmann, U., Kawamura, K., 2015. North Atlantic Holocene climate evolution recorded by high-resolution terrestrial and marine biomarker records. Quaternary Science Reviews 129, 111-127.

* Corresponding Author; Tel: +44-(0)-121-4146139; e-mail: h.moossen@bham.ac.uk

Abstract

Holocene climatic change is driven by a plethora of forcing mechanisms acting on different time scales, including: insolation, internal ocean (e.g. Atlantic Meridional Overturning Circulation; AMOC) and atmospheric (e.g. North Atlantic Oscillation; NAO) variability. However, it is unclear how these driving mechanisms interact with each other. Here we present five, biomarker based, paleoclimate records (air-, sea surface temperature and precipitation), from a fjordic sediment core, revealing North Atlantic terrestrial and marine climate in unprecedented detail. The Early Holocene (10.7 - 7.8 kyrs BP) is characterised by relatively high air temperatures while SSTs are dampened by melt water events, and relatively low precipitation. The Middle Holocene (7.8 - 3.2 kyrs BP) is characterised by peak SSTs, declining air temperatures and high precipitation. A pronounced marine thermal maximum occurs between ~ 7 - 5.5 kyrs BP, 3000 years after the terrestrial thermal maximum, driven by melt water cessation and an accelerating AMOC. The neoglacial cooling, between 5.8 and 3.2 kyrs BP leads into the late Holocene. We demonstrate that an observed modern link between Icelandic precipitation variability during different NAO phases, may have existed from ~7.5 kyrs BP. A simultaneous decoupling of both air, and sea surface temperature records from declining insolation at ~3.2 kyrs BP may indicate a threshold, after which internal feedback mechanisms, namely the NAO evolved to be the primary drivers of Icelandic climate on centennial time-scales.

1. Introduction

A multitude of paleoclimate reconstructions show that the climate of the Holocene, the last ~11.5 kyrs (kilo years), has been far from stable (Bond et al., 2001; Mayewski et al., 2004; Wanner et al., 2011). Prominent climate events include the Holocene thermal maximum (HTM; Kaufman et al., 2004), the 8.2 event (Alley and Ágústsdóttir, 2005), the neoglacial period (Jennings et al., 2002), the Medieval Climate Anomaly (MCA; Graham et al., 2011) and the Little Ice Age (LIA; Ogilvie and Jonsson, 2001). The latter climate events have had significant impacts on human societies (Buntgen et al., 2011; D'Andrea et al., 2011; deMenocal, 2001).

Holocene climatic change is attributed to a plethora of climatic drivers acting on different time scales (Mayewski et al., 2004; Wanner et al., 2011). The overarching external climate driver throughout the Holocene is the changing geometry of Earth's orbit around the sun, which over the last ~ 11 kyrs has driven decreasing summer insolation in the northern hemisphere (Laskar et al., 2004). This orbital cycle affects the climate on millennial and longer time scales by, for example, driving latitudinal shifts of the polar front and the Intertropical Convergence Zone (ITCZ; Haug et al., 2001; Knudsen et al., 2011). Superimposed on this lower-frequency orbital climate driver, higher-frequency volcanic activity and changes in the sun's intensity influence climate on annual to millennial timescales (Gray et al., 2010; Wanner et al., 2011). For example, the Maunder (solar) minimum contributed to the cooler climate of the LIA (Shindell et al., 2001), and recent models link solar activity with climate phenomena such as the North Atlantic Oscillation (Ineson et al., 2011).

The North Atlantic Oscillation (NAO) is the main driver of temperature and precipitation variability in the North Atlantic and Europe (Hurrell, 1995; Hurrell et al., 2003). The NAO describes the strength and directional changes of the westerlies traversing the North Atlantic (Hurrell, 1995). When the NAO is in positive mode (NAO+), westerlies bring moist and warm air masses to Northern Europe (Fig. 1c), while southerly trending westerlies drive a drier and colder climate in Northern Europe when the NAO is in negative mode (NAO-; Hurrell et al., 2003; Fig. 1d). Contemporary observations indicate that the NAO operates over annual to decadal time scales (Hurrell, 1995; Hurrell et al., 2003). However, recent paleoclimate reconstructions show that atmospheric variations, attributed to NAO-type variability, have operated on centennial and even millennial time scales (Olsen et al., 2012; Trouet et al., 2009; Figs. 6h, i), contributing to prominent climatic events such as the MCA and the LIA (Trouet et al., 2009). Shifting NAO phases also influence the relative strength of the Irminger and North Icelandic Irminger Currents (IC and NIIC) in the Denmark Strait (Blindheim and Malmberg, 2005), whereby more warm, saline Atlantic Water flows through the Denmark Strait during NAO+, compared to NAO- phases (Figs. 1e, f).

The IC and NIIC are part of a network of currents contributing to the Atlantic Meridional Overturning Circulation (AMOC; Hansen and Østerhus, 2000; Vage et al., 2011). The AMOC mediates a significant amount of the pole-ward energy transfer in the northern Hemisphere and contributes to the current mild Northern European climate (Broecker, 1997). Changes in the intensity of the AMOC have been linked to changes in deep water production as indicated by velocity variations of Iceland Scotland Overflow Waters (Hall et al., 2004; Fig. 6k).

The solar, atmospheric and oceanic forcing mechanisms described above are some of the drivers that have been invoked to explain the climate evolution of the Holocene (Bond et al., 2001; Harrison et al., 1992; Mayewski et al., 2004). However, the interactions of these climatic drivers, their relative importance, and the time scales on which they operate are still not well understood. This knowledge gap is evident when considering Bond cycles, which were first described nearly two decades ago (Bond et al., 1997; Fig. 6g). Bond cycles are defined as cyclical (~ 1500 ± 500 years) penetrations of cold surface water, accompanied by drift ice, into the southeast North Atlantic (Bond et al., 1997). Such cycles are thought to be, at least in part, driven by changes in the sun's intensity (Bond et al., 2001). However, other driving mechanisms such as changes in the intensity of the AMOC, changing meridional atmospheric circulation, enhanced regional upwelling, changes in polar water fluxes and NAO indices have also been invoked as possible drivers of Bond cycles (Wanner et al., 2011; and references therein). Despite the number of driving mechanisms that are thought to cause Bond cycles, evidence of these events is not observed in all northern hemisphere paleoclimate records, and many paleoclimate records only show some, and not all of the Bond cycles (Wanner et al., 2011). For example, North Icelandic Shelf diatom and alkenone based sea surface temperature (SST) reconstructions do not show Bond cycles (Bendle and Rosell-Melé, 2007; Justwan et al., 2008; Fig. 6j), even though one might expect distinct N. Atlantic cold SST episodes to be recorded in Holocene sediments from the Icelandic margin.

Iceland and its surrounding waters have received significant scientific attention because climatic archives found in the area integrate proxy responses to most, if not all, climatic forcing mechanisms that have affected Holocene climate in the North Atlantic sector (Andrews and Jennings, 2014; Axford et al., 2011; Geirsdottir et al., 2002; Jennings et al., 2011; Quillmann et al., 2010; Quillmann et al., 2012). Consequently we present five new high-resolution paleoclimate records (n = 326; 1 sample/~30 years; Figs. 6a - e) covering the period between ~10.7 and ~0.3 calibrated kilo years before present (kyrs BP) from a single sediment core (MD99-2266) from Ísafjarðardjúp fjord in the Denmark Strait (Figs. 1a, b). Fjords are conducive to high sedimentation rates (Howe et al., 2010), facilitating high-resolution paleoclimate reconstructions. Moreover, since fjords bridge the land-ocean interface, paleo-environmental records from fjords provide a unique opportunity to study the link between marine and terrestrial climate. Our five new, biomarker based, reconstructions of three key climatic variables (SST, air temperature and precipitation) represent the most diverse array of marine and terrestrial, high-resolution paleoclimate signals extracted from a single marine archive thus far. The fact that all records are derived from a single sediment core allows their direct comparison without the potential bias inherent to different age models.

The multi-proxy approach is being facilitated by an expanding organic biomarker "toolbox" that enables paleoclimatologists to produce increasingly comprehensive climate reconstructions from a variety of climatic archives (Castañeda and Schouten, 2011; Eglinton and Eglinton, 2008). Here we use this approach to address the following question: to what extent and on what time scales have various climate forcing mechanisms influenced Icelandic SST, MAT and precipitation regimes?

2. Materials and Methods

2.1. Core Location and Oceanography

The Calypso piston core MD99-2266 was retrieved from the mouth of Ísafjarðardjúp fjord, Northwest Iceland (66° 13’77’’ N, 23° 15’93’’ W; Figs. 1a, b), from 106 m water depths, during Leg III of the 1999 IMAGES V cruise aboard the R/V *Marion Dusfresne* (Quillmann et al., 2010 and references therein). It has a 10 cm diameter and a length of 3890 cm.

Ísafjarðardjúp fjord is the largest fjord of the Vestfirdir Peninsula. It is ~90 km long and 10 to 15 km wide. Together with its tributary fjords, it covers an area of ~1150 km^2 and drains ~2300 km^2 (Andrews et al., 2008). The Drangajökull icecap is located in the north eastern highlands of Vestfirdir Peninsula and its melt waters flow into Ísafjarðardjúp fjord and into Jökullfirðir, which is the largest tributary fjord of Ísafjarðardjúp (Andrews et al., 2008).

The core site is affected by two surface currents. The IC is the most westerly water current of the North Atlantic that brings warm Atlantic Water into the Nordic Seas. Today, the volume flux of the IC is estimated to be one Sverdrup (1 SV = 10^6 m^3 s^{-1}) and its heat flux (relative to 0 °C) is estimated to be 25 Terra Watts (Hansen and Østerhus, 2000). The IC enters the Denmark Strait and divides into two branches. The NIIC branches off towards the east where it flows onto the North Icelandic Shelf. The second branch flows southwest along the Greenland coast, parallel to the East Greenland Current (EGC; Hansen and Østerhus, 2000). The Polar Front (PF) separates the warm and saline waters carried north by the IC from the colder and fresher polar waters which are carried south by the EGC (Jennings et al., 2011). The location of the PF is determined by the relative strengths of these warm and cold water currents (Ólafsdóttir et al., 2010).

2.2. Age model and Sampling Strategy

The age model of MD99-2266 that was previously published by Quillmann et al. (2010) is used here. It consists of 24 ^{14}C-AMS (Accelerated Mass Spectrometry) dated bivalve and benthic foraminifera shells, as well as the Saksunarvatn tephra, which is located at a sediment depth of 3591 cm (Fig. 2). Quillmann *et al*. (2010) omitted 5 ^{14}C-AMS dates because the dates are older than the underlying dated horizons. Three of those dates are in the top 23 cm suggesting that the core top sediments were disturbed (Quillmann et al., 2010). Quillmann et al. (2010) did not apply an ocean reservoir correction. The mean (2σ standard deviation) error associated with the 19 14C-dates that were used for the final age model, and the Saksunarvatn tephra layer, is ± 165 calibrated years. Following Moossen et al. (2013), sample ages were calculated assuming linear sedimentation rates (shown in Fig. 2) between each 14C-AMS dated sediment horizons and between the youngest 14C-AMS date and the core top.

Depending on the amount of available sediment, a minimum of 1 cm^3 and a maximum of 6 cm^3 of sediment were sampled from each time horizon. Where the piece of sediment representing a sample of a desired time interval was longer than 6 cm, an equal amount of sediment was taken from the beginning, the middle and the end of the sediment package representing one sample (time) interval. A total of 326 sediment samples were collected.

2.3. Sample preparation and analyses

The methods for sample preparation and biomarker analyses are identical to the ones previously described by Moossen et al. (2013). Samples were solvent extracted using dichloromethane/methanol (3:1 v/v). An internal standard consisting of Squalane, 2-Nonadecanone, 1-Nonadecanol and Eruic acid was added to each sample. Samples were fractionated using silica gel column chromatography following Bendle et al. (2007).

A gas chromatograph (GC; Shimadzu 2010) with a flame ionisation detector (FID) and a Shimadzu OP2010-Plus Mass Spectrometer (MS) interfaced with a Shimadzu 2010 GC were used for the quantitative and qualitative analysis of alkenones and *n*-alkanes (Moossen et al., 2013). Compound separation was achieved using one of two identical columns, either a BP1 (SGE Analytical Science) or a TG-1MS (Thermo

Scientific) column (60m, diameter: 0.25 mm, film thickness: 0.25 µm; coating: 100 % Dimethyl-polysiloxane). The GC oven was held at 60 °C for two minutes, then the temperature was ramped up to 120 °C at 30 °C min^{-1} and then to 350 °C at 3 °C min^{-1}, where the temperature was held for 20 minutes. An injection standard consisting of methyl behenate was co-injected with each sample.

The relative tetraether abundances in 299 MD99-2266 sediment samples were analysed using high performance liquid chromatography-atmospheric pressure chemical ionisation-mass spectrometry (HPLC-APCI-MS) at the Organic Geochemistry Unit at the University of Bristol. Tetraether analysis was identical to that previously described in Moossen et al. (2013).

The hydrogen isotopic measurements of the C_{29}-*n*-alkane in 133 samples were conducted at the Institute of Low Temperature Science at the Hokkaido University, Japan. The isotopic values are expressed as per mil (‰; Eq. 1; vs. Standard Mean Ocean Water (SMOW).

$$\delta(‰)=((R_{sample}-R_{standard})/(R_{standard}))x1000 \qquad \text{Eq. 1}$$

The hydrogen isotopic signature of the C_{29}-*n*-alkane (δD_{C29}) was analysed using an HP 6890 GC interfaced with a Finnigan MAT Delta Plus XL MS. The Finnigan MAT combustion furnace was held at 1450 °C. The chromatographic separation of the *n*-alkanes was accomplished using a DB5-HT column (Agilent J&W GC Columns; 30 m, 0.25 mm diameter; 0.1 µm film thickness). The following GC oven temperature program was used: the temperature was ramped up from 50 to 120 °C at 10 °C min^{-1}, and then to 310 °C at 4 °C min^{-1}, where the temperature was held for 20 minutes. An external standard consisting of an *n*-alkane mix (C_{16} - C_{30}) with a known hydrogen isotopic composition was injected daily to evaluate the measurement drift of the instrument and ensure analytical precision. The isotopic composition of the C_{29}-*n*-alkane and of the internal standard (Squalane) was calculated relative to the isotopic composition of an injection standard (Methyl Eicosanoate; δD: -226.8 ‰ vs SMOW) that was co-injected with each sample. The δD value of the internal standard squalane is -179.5 ± 4.7 ‰ (the uncertainty describes the 1σ standard deviation (SD) of squalane in 133 samples over the entire time of analyses). 28 samples were analysed in duplicate and 2 in triplicate, and the 1σ SD of the C_{29}-*n*-alkane relative to the injection standard was ± 3.5 ‰. However, as not all samples were analysed in duplicate due to low *n*-alkane concentrations, we use the internal standard squalane that is present in all 299 samples to determine the analytical precision of the measurements.

2.4. Biomarker and statistical analyses

$U^{K'}_{37}$-SSTs (Fig. 6a) were reconstructed from 326 samples using the relative abundance of the C_{37}-alkenones with two ($C_{37:2}$) and three ($C_{37:3}$) double bonds. Relative abundances were converted into $U^{K'}_{37}$-values after Prahl and Wakeham (1987; Eq. 2). The $U^{K'}_{37}$-values were converted to SSTs using the calibration equation published by Conte et al. (2006; Eq. 3).

$$U^{K'}_{37} = C_{37:2}/(C_{37:2} + C_{37:3}) \qquad \text{Eq. 2}$$

$$SST = (U^{K'}_{37}-0.0709)/0.0322 \qquad \text{(calibration error of 1.1 °C)} \qquad \text{Eq. 3}$$

Thirty-four samples were analysed in triplicate and the mean analytical error (1σ SD) associated with the $U^{K'}_{37}$ index is ± 0.01 which translates into a temperature uncertainty of ± 0.44 °C.

The mean air temperatures (MATs) of 299 samples were reconstructed based on the relative abundance of branched glycerol-dialkyl-glycerol-tetraethers (br-GDGTs; Peterse et al., 2012; Weijers et al., 2007b). The cyclisation ratio (CBT, Eq. 4), and the methylation index of branched tetraethers (MBT', Eq. 5; Peterse et al., 2012) are converted to CBT/MBT'-MATs using the calibration equation published by Peterse et al. (2012; Eq. 6).

$$CBT = -\log([Ib + IIb] / [Ia + IIa]) \quad \text{Eq. 4}$$

$$MBT' = ([Ia + Ib + Ic]) / ([Ia + Ib + Ic]+[IIa + IIb + IIc] + [IIIa]) \quad \text{Eq. 5}$$

$$MAT = 0.81 - 5.67 \times CBT + 31.0 \times MBT' \quad \text{(root mean square error of 5 °C)} \quad \text{Eq. 6}$$

The roman numerals in equations 3 and 4 refer to the relative abundance of the br-GDGT molecules (Fig. S3; SI 2). Nine samples were analysed in triplicate and two in duplicate and the 1σ SD associated with the CBT/MBT'-MAT measurements is ± 0.5 °C.

Soil pH variations were reconstructed using the revised calibration equation published by Peterse et al. (2012; Eq. 7).

$$pH=7.90-1.97 \times CBT \quad \text{(root mean square error of 0.8 pH units)} \quad \text{Eq. 7}$$

Nine samples were analysed in triplicate and two in duplicate and the 1σ SD associated with the soil pH measurements is ± 0.04 pH units.

Following Moossen et al. (2013), Average chain length (ACL_{25-35}) values from 310 samples were calculated using the concentrations of the most abundant odd-chained *n*-alkanes with 25 to 35 carbon atoms (Eq. 8; Schefuss et al., 2003). While Moossen et al. (2013) used the ACL_{25-35} record to identify 16 samples as outliers (see also Fig. S2; SI

2), the ACL_{25-35} record, without the 16 outliers is published here and interpreted as showing precipitation change (see discussion below).

$$ACL_{25-35}=(\Sigma(X_i \times C_i)_n)/(C_i)_n \qquad \text{Eq. 8}$$

X_i represents the *n*-alkanes and C_i represents the abundance of the *n*-alkanes. 11 samples were analysed in triplicate and the mean 1σ SD associated with the ACL_{25-35} values is ± 0.06.

The C_{29}-*n*-alkane was abundant enough for hydrogen isotopic analysis in 133 samples. The δD_{C29} values were corrected for the influence of the global ice volume on the hydrogen isotopic composition of meteoric water following Collins et al. (2013) and Niedermeyer et al. (2010) by using the benthic foraminifera oxygen isotope curve published by Waelbroeck et al. (2002; Fig. S1, SI 2). First, the uncorrected δD_{C29} value were converted to $\delta^{18}O$ values using the meteoric water line equation published by Craig (1961). Then the $\delta^{18}O$ value of each sample was corrected for the influence of ice volume using the 3rd order polynomial equation (Fig. S1, SI 2). Finally, the $\delta^{18}O$ values of the samples were converted back into global ice volume corrected δD_{C29} values (Fig. 3).

REDFIT spectral analyses were conducted using PAST (Hammer et al., 2001; Fig. 7). REDFIT spectral analyses can be performed on unevenly spaced time series (Schulz and Mudelsee, 2002). This pre-empts the need for regular interpolation of the time series presented in this paper. An AR(1) red noise model and the 95 % confidence threshold is fitted to each spectral analyses.

3. Results and Discussion

3.1. Paleoclimate proxies

The $U^{K'}_{37}$-SST proxy is based on variations of $C_{37:2}$ and $C_{37:3}$-alkenones produced by certain haptophyte algae (e.g. *Emiliania huxleyi*) as a response to changing SSTs (Brassell et al., 1986). Previous studies have shown that the $U^{K'}_{37}$-index can be used to reconstruct SSTs on the Icelandic Shelf (Bendle and Rosell-Melé, 2007; Sicre et al., 2011). The $U^{K'}_{37}$-SSTs reported here tend to be higher than those reported previously on the North Icelandic Shelf (Bendle and Rosell-Melé, 2007; Sicre et al., 2011; Fig. 7h). Presumably this is due to the more southerly location of the Ísafjarðardjúp fjord with waters dominated by the warm IC and NIIC (Figs. 1e, f). Additionally, $U^{K'}_{37}$-SSTs are likely biased towards summer due to the predominant production of alkenones during summer months at high latitudes, as suggested for the Icelandic Shelf (Bendle and Rosell-Melé, 2007; Sicre et al., 2008b), the Southern Ocean (Sikes et al., 1997; Ternois et al., 1998) and the Gulf of Alaska (Prahl et al., 2010). This is seemingly confirmed by the close match between core top and mean local summer June/July/August (JJA) SST of 9.6 °C at Stykkishólmur from 1867-1985 (Hanna et al., 2006; Fig. 6a). We assume that most of the sedimentary alkenones are produced locally and note that previous work demonstrates that potential mixing of allochthonous with *in situ* produced alkenones does not disturb the $U^{K'}_{37}$-SST relationship significantly on the Icelandic shelf (Bendle and Rosell-Melé, 2004).

Holocene $U^{K'}_{37}$-SSTs fluctuate between 6.6 °C at ~1.1 kyrs BP, and 14.8 °C at ~7.3 kyrs BP. The mean SST throughout the early Holocene is 10 °C. At the transition from the early to the middle Holocene, the amplitude of SST variability increases, and the onset of the middle Holocene sees the highest reconstructed SSTs (14.8 °C at ~7.3

kyrs BP). Between ~5.9 and ~3.2 kyrs BP SSTs decrease from 13.5 to 6.7 °C before rising again during the late Holocene. The mean SST during the late Holocene is 8.9 °C, but with significant variability around the mean throughout the last 2000 years of the record.

The CBT/MBT'-MAT reconstruction (Fig. 6b) is based on the variable abundances of br-GDGTs synthesised by subdivisions of *Acidobacteria* (Sinninghe Damsté et al., 2011) and other unspecified soil bacteria (Peterse et al., 2012; Weijers et al., 2007b). There is evidence that br-GDGTs are not amenable to aeolian transport (Gao et al., 2012), indicating that paleo proxies based on these compounds likely reflect a proximal Icelandic signal. The CBT/MBT'-MAT proxy is based on the assumption that br-GDGTs are exclusively produced by terrestrial organisms. Recent work suggests that br-GDGTs may have an aquatic source as well (Fietz et al., 2012), although direct evidence of such a source is still missing (Rueda et al., 2013). The CBT/MBT'-MATs in this study are mainly controlled by variations of just one br-GDGT compound. Throughout the Holocene, the relative concentration of br-GDGT IIIa increases from ~ 10 % to ~ 45 %, while the concentration of the other br-GDGTs remains relatively stable through time (SI 2; Fig. S4). The relative abundance of br-GDGT IIIa tracks changes of the previously published BIT-index closely (Fig. 4; Moossen et al., 2013). The BIT-index indicates changes in terrestrial soil input (Hopmans et al., 2004), and has been shown to yield reliable soil input results for Ísafjarðardjúp fjord (Moossen et al., 2013). This infers that GDGT IIIa is mainly derived from local Icelandic soils. Furthermore, previous studies have shown that the relative abundance of br-GDGT IIIa does not change significantly when comparing soils/near shore settings with open marine settings (Peterse et al., 2009; Zhu et al., 2011). These findings suggest that the primary climatic signals, CBT/MBT'-MAT, and also soil pH (see below), are preserved and not confounded by any changes in terrestrial sediment, or marine vs. terrestrial source dynamics of Ísafjarðardjúp fjord and its catchment area.

Reconstructed CBT/MBT'-MATs follow decreasing Holocene summer insolation closely (r^2 = 0.84; Fig. 5). Therefore we hypothesise that the primary control on CBT/MBT'-MAT is summer insolation change in this study. The close match between core top reconstructed temperatures and the mean instrumental summer air temperature (JJA) of 9.3 °C at Stykkishólmur from 1878-2002 (Fig. 6b; Hanna et al., 2004) seemingly supports the hypothesis that the CBT/MBT'-MATs represent summer season, rather than mean annual temperatures. Furthermore, the reconstructed CBT/MBT'-MATs of the most recent ~1.8 kyrs BP are in good agreement with reconstructed August air temperatures based on chironomid assemblages from north Iceland (Axford et al., 2009; Fig. 7). Finally, even though no clear evidence of a seasonal bias of the CBT/MBT'-MAT proxy has been found in soils at mid-latitudes (Weijers et al., 2011), studies conducted in the Skagerrak (58° N; Rueda et al., 2009) and in Arctic lakes (50° - 73°N; Shanahan et al., 2013) suggest that the CBT/MBT'-MAT proxy represents summer, rather than mean annual temperatures at high latitudes. Both, Rueda et al. (2009) and Shanahan et al. (2013) suggest that the bias towards summer season temperatures may be due to the br-GDGT producing soil bacteria being more active in the summer, when the soils are not frozen or snow covered. Since the calibration equation developed by Weijers et al. (2007b), and refined by Peterse et al. (2012) correlates br-GDGT variability with mean annual temperature (and no alternative summer-season CBT/MBT calibration is currently available), we continue to use CBT/MBT'-"MAT" in the text when referring to the br-GDGT air temperature changes, but we interpret the signal as weighted towards the summer, rather than mean annual temperatures.

The mean reconstructed Holocene CBT/MBT'-MAT is 11.8 °C. The highest CBT/MBT'-MAT of 16.6 °C is observed at 9.7 kyrs BP, and the lowest CBT/MBT'-MAT of 7.2 °C is observed at 540 yrs BP. The highest CBT/MBT'-MATs throughout the early Holocene are interrupted by a ~5 °C temperature drop between ~9.7 and ~9 kyrs BP. Subsequently MATs continually decrease from 16.5 °C at ~9 kyrs BP to 8.1 °C at ~3 kyr BP. Throughout the late Holocene, MATs fluctuate around a mean summer temperature of 9.5 °C.

Three independent qualitative approaches are presented here to estimate changes in precipitation. Firstly, we infer precipitation variability from soil pH changes that are reconstructed based on br-GDGTs variability (Peterse et al., 2012; Weijers et al., 2007b; Fig. 6c). Soil leaching processes result in soil acidification when precipitation is high (Johnson et al., 1998). The absolute soil pH values presented here suggest more alkaline soil types compared the dominant Icelandic soil type, andosol (Arnalds, 2008). Peterse et al. (2010) have shown that the br-GDGT proxy overestimates absolute soil pH values when applied to acidic soils, such as andosol (Arnalds, 2008). Therefore, we do not interpret absolute soil pH values, but rather temporal trends that are indicative of relative pH changes, driven by precipitation variability (Fawcett et al., 2011; Weijers et al., 2007a). As discussed previously, the br-GDGT based CBT/MBT'-MAT proxy likely records a summer season, rather than annual signal, possibly due to increased soil bacterial activity during the summer at high latitudes (Rueda et al., 2009; Shanahan et al., 2013). Consequently, it is likely that the br-GDGT based soil pH proxy also records a summer signal.

Secondly, we present two independent proxies based on higher plant wax derived *n*-alkanes that respond to precipitation change. *n*-Alkanes comprise part of the protective wax layer that coats leaves (Eglinton et al., 1962). They are transported via aeolian and fluvial mechanisms into marine sediments and preserved over geological time periods (e.g. Eglinton and Eglinton, 2008, and references therein). Due to the proximity of the core location to land we suggest that the majority of the terrigenous material is derived from the catchment area of Ísafjarðardjúp fjord, likely transported during the spring melt following the winter snowfall maxima that is observed in modern Icelandic annual precipitation (Hanna et al., 2004).

The temporal variability of dominant (preferentially produced) leaf wax *n*-alkanes ($ACL_{25\text{-}35}$) is controlled by: contributing plant types (e.g. Rommerskirchen et al., 2006b), ambient air temperature (Kawamura et al., 2003; Vogts et al., 2012) and precipitation regime (e.g. Calvo et al., 2004). The $ACL_{25\text{-}35}$ record presented here exhibits shifts of ~0.5 $ACL_{25\text{-}35}$ units at the transition from the early to the middle, and again from the middle to the late, and throughout the late Holocene (Fig. 6d). These shifts are remarkably large and occur over comparatively short time scales. Elsewhere, similar average chain length shifts have been associated with large scale changes from C_3 vegetation dominated landscapes to C_4 vegetation dominated landscapes (and vice versa) over glacial/interglacial time scales (Badewien et al., 2015; Calvo et al., 2004; Rommerskirchen et al., 2006a). Pollen studies from lake sediments and peat deposits show dynamic vegetation variability in Iceland throughout the Holocene. Vestfirdir peninsula vegetation was dominated by Cyperaceae (herbs) and Poaceae (grasses) with small amounts of *Salix*, *Juniperus* and *Betula* (birch) throughout the last 10,000 kyrs BP (Caseldine et al., 2003). *Betula* pollen first occured between 7.8 and 7 kyrs BP but never increased above 20 % of the total land pollen sum throughout the pollen record (Caseldine et al., 2003). Elsewhere in northern Iceland birch woodland also became more abundant, until ca. 1000 yrs BP, when it declined again following the settlement of Iceland (Hallsdottir, 1995). Trees produce more short chained *n*-alkanes than grasses (Rommerskirchen et al., 2006b; Vogts et al., 2009). Therefore, it is possible that an increase in the amount of *betula* pollen did contribute to the decreasing $ACL_{25\text{-}35}$ values between 7.8 and 7 kyrs BP. However, it is unlikely that the advent of the *betula* occurrence alone is responsible for the large shifts in $ACL_{25\text{-}35}$ throughout the record. Furthermore, pollen abundances from lake Vatnskotsvatn (northern Iceland) do not show major variations in the relative amounts of different types of plants (trees, grasses, herbs) between 3.2 and 1 kyr BP (Hallsdottir, 1995), during which time we observe large $ACL_{25\text{-}35}$ shifts (of an amplitude equivalent to that observed between 7.8 and 7 kyrs BP). Therefore, we suggest that changes in vegetation are not the main driver for $ACL_{25\text{-}35}$ shifts observed in MD99-2266 (Fig. 6d).

CBT/MBT'-MAT and $ACL_{25\text{-}35}$ co-vary throughout the late Holocene suggesting that temperature change may have influenced the leaf wax *n*-alkane distribution over the last 3000 yrs BP. However, no clear linear relationship between the CBT/MBT'-MAT and the $ACL_{25\text{-}35}$ records is observed for the entire Holocene (r^2 = 0.1; n = 285) suggesting that temperature is not the main driver for changes in the *n*-alkane distribution. While the linear correlation between the $ACL_{25\text{-}35}$ and soil pH records (r^2 = 0.2; n = 285) is only marginally stronger, the long term co variation of the $ACL_{25\text{-}35}$ and the soil pH record suggests that the $ACL_{25\text{-}35}$ responds to changes in precipitation. Assuming that leaf waxes are produced during the main growing season of plants at high latitudes, they likely record spring/summer, rather than annual precipitation.

The hydrogen isotopic composition of the C_{29}-*n*-alkane (δD_{C29}) is used as an additional proxy for precipitation change (Fig. 6e). The photosynthesis of organic matter by terrestrial higher plants utilizes soil water that ultimately derives from precipitation

(Sachse et al., 2012). The hydrogen isotopic compositions of leaf wax derived *n*-alkanes consequently reflect changes in precipitation and are an established proxy to reconstruct paleo-precipitation regimes (Sachse et al., 2012; Schefuss et al., 2005). The spatial and temporal isotopic variability of precipitation is controlled by hydrological variables, the continental, temperature and amount effects, and these need to be considered when interpreting the δD_{C29} isotopic signature (Sachse et al., 2012). For at least the last 1000 years, the amount of precipitation Iceland receives has been driven by the NAO (Hurrell, 1995; Trouet et al., 2009). Iceland receives more precipitation during NAO+, compared to NAO- phases (Hurrell, 1995). The close link between the NAO and precipitation amounts suggests that the main moisture source for Icelandic precipitation is the moisture transported by the westerly storm track that traverses the North Atlantic (Figs. 1c, d). While the latitudinal trajectory and the strength of these westerlies has decreased throughout the Holocene, their direction has remained the same (Harrison et al., 1992), suggesting that the hydrogen isotopic variability observed here cannot be attributed to major changes in water source areas. Therefore, we postulate that the δD_{C29} variability in the studied area reflects shifting NAO modes due to different precipitation regimes at least in the late Holocene. In the early Holocene, relatively high temperatures likely also influenced the isotopic signature of leaf wax components and will be discussed later.

The soil pH, $ACL_{25\text{-}35}$ and δD_{C29} proxies all show remarkably similar millennial to centennial variability, particularly in the late Holocene (Figs. 6 and 7c, d, e). Therefore, we are confident that the interpretation of all three proxies in concert allows a robust interpretation of relative changes in precipitation.

The average proxy values spanning the Holocene are 7.9 for soil pH, 29.12 for ACL_{25-35}, and -197 ‰ for δD_{C29} (Figs. 6c, d, e). The combined precipitation proxy records tend towards less than average precipitation from ~10.7 to 7.8 kyrs BP, increased precipitation from ~7.8 to ~3 kyrs BP and considerable fluctuation around the mean throughout last 3 kyrs BP of the records.

3.2. Comparing terrestrial and marine biomarker records

Magnetic susceptibility data from Ísafjarðardjúp and its tributary fjords shows that the post glacial sedimentation history has been very dynamic (Andrews et al., 2008). For example, high concentrations of magnetic minerals in early Holocene sediments reflect the final deglaciation of Iceland (Andrews et al., 2008). Such a dynamic sedimentation history has also been inferred through changing inputs of terrestrial vs. marine organic matter into Ísafjarðardjúp (Moossen et al., 2013). Moossen et al. (2013) argue that the build-up of soil and plant biomass in the aftermath of deglaciation, and subsequent soil erosion during the Neoglacial, and settlement of Iceland, led to a ~10 % increase in sedimentary terrestrial organic matter content in Ísafjarðardjúp ford from the early, through the middle, into the late Holocene. Dynamic erosion and sedimentation of terrestrial organic matter throughout the late Holocene has also been described in lake Haukadalur (Geirsdottir et al., 2009b), which lies just south of the Vestfirdir Peninsula. It is conceivable, as is the case in lake Haukadalur (Geirsdottir et al., 2009b), and in a Canadian fjord (Smittenberg et al., 2006), that increased sedimentation of terrestrial organic matter in the late Holocene, may have led to the deposition of a mix of fresh and old biomarkers. However, the comparison of the terrestrial biomarker data with other palaeoclimate records (see discussion below) clearly indicates that the biomarkers analysed in this study record climatic events. For example, the CBT/MBT'-MAT proxy follows declining insolation in the early, and middle Holocene. Additionally, when comparing the five biomarker records to palaeo-NAO reconstructions (Olsen et al., 2012; Trouet et al., 2009) the records collectively show a synchronous response (see discussion below). Thus, the palaeoclimate records presented here indicate that the influence of old/reworked organic carbon was not significant enough to confound primary climatic signals.

Many of the conclusions drawn from the five biomarker records presented in this paper are based on the assumption that the temporal offset between the production and sedimentation of the different biomarkers does not exceed the resolution of the biomarker records. The integral prerequisite to this assumption is that the time it takes for the studied biomarkers to be transported from their respective precursor organisms into the sediment is similar enough that the interpreted signals indeed reflect the same climate events. Even if lateral transport of a small portion of alkenones is assumed, alkenones still have the most direct transport pathway into marine sediments compared to terrestrially derived br-GDGTs (Gao et al., 2012), that are thought to be mainly transported via fluvial mechanisms, and higher plant wax *n*-alkanes, that are transported via aeolian and fluvial mechanisms (e.g. Eglinton and Eglinton, 2008, and references therein). Here too, the synchronous response of the five biomarker records to NAO variations in the late Holocene suggests that the transport times of different biomarkers to the sediment are at least similar enough to resolve centennial scale climatic changes.

4. <u>Holocene climate evolution</u>

The five combined paleoclimate records from Ísafjarðardjúp fjord reveal terrestrial and marine climate in unprecedented detail for a marine sediment core record covering the entire Holocene (Figs. 6a-e). The combination of proxy records allows the placement of new constraints on the relative importance of different climatic drivers for Icelandic climate throughout the Holocene. Below we discuss how the climate of the early, middle and late Holocene was likely driven by the changing relative influence of large-scale climatic drivers.

Concerted inspection of the $U^{K'}_{37}$-SST, the CBT/MBT'-MAT, and the precipitation records highlight two noteworthy and distinct climatic shifts at ~7.8 and ~ 3.2 kyrs BP (Fig. 6). No one individual proxy record clearly delimits these phase shifts, which is expected as individual proxies are recording marine or terrestrial temperatures or precipitation. These climatic parameters inherently have differential responses and sensitivity to external drivers and internal climate forcing mechanisms. Even in the case of the three proxies which record precipitation, different biogeochemical (biosynthesis of lipids) and physical processes (isotopic fractionation) are involved in transcribing the climatic signal, with a varying degrees of fidelity.

In the following section we will discuss the competing driving mechanisms that likely drove the climatic shifts at ~7.8 and ~3.2 kyrs BP. We explore the changing relative importance of the climate drivers, as they shaped the three distinct climatic periods of the Holocene.

4.1. Early Holocene and glacial aftermath (10.7 to 7.8 kyrs BP)

The CBT/MBT'-MAT reconstruction indicates that Icelandic terrestrial air temperatures were considerably warmer during the early Holocene than at any other time covered by the record (Fig. 6b). This observation is synchronous with a maxima in high northern hemisphere summer insolation (Laskar et al., 2004). Indeed, it is the close correlation between the reconstructed CBT/MBT'-MATs and summer insolation throughout the early and the middle Holocene, which indicates that summer insolation was the main driver for summer season terrestrial climate (Fig. 5). The CBT/MBT'-MAT record also reveals that the terrestrial Holocene thermal maximum occurred between ~10.5 and ~8.5 kyrs BP. This timing broadly agrees with chironomide based temperature reconstructions, which indicate a terrestrial warm period between ~10.5 and 7.5 kyrs BP (Caseldine et al., 2003; Langdon et al., 2010). Increased primary production in lake Hvítárvatn also indicate warm summers between 10.2 and 9 kyrs BP (Larsen et al., 2012). Interestingly, there is no clear 8.2 kyr signal in the climate records presented here, compared to the GISP 2 oxygen isotope record (Grootes and Stuiver, 1997; Fig. 6i). The CBT/MBT'-MAT does drop during the period coinciding with the 8.2 kyr event, but the decrease is not significant when viewed in context of the early (and entire) Holocene record (Fig. 6b). Our sample resolution (27 samples between 8 - 8.4 kyrs BP: 1 sample/~15 yrs BP), is sufficient to capture the 8.2 kyr event, which lasted for *ca.* 400 years (Alley and Ágústsdóttir, 2005). However, there is only one data point within the period of the 8.2 kyr event that shows a noteworthy CBT/MBT'-MAT decrease. This suggests that either a) the 8.2 kyr event did not exert a significant influence on Icelandic terrestrial climate, or b) the CBT/MBT'-MAT proxy does not record it. The latter explanation is most likely, given that, numerous records suggest a significant impact of the 8.2 kyr event on climate in the North Atlantic sector (Alley and Ágústsdóttir, 2005; Quillmann et al., 2012; Rohling and Palike, 2005). Rohling and Palike (2005) find evidence that paleoclimate proxies biased towards summer seasons, do not record the 8.2 kyr event clearly. This is consistent with the CBT/MBT'-MAT proxy that likely records summer, rather than mean annual temperature at high latitudes (see discussion above).

$U^{K'}_{37}$-SSTs do not show a clear relationship with insolation during the early Holocene (Fig. 6a). Indeed, while summer insolation peaked throughout the first 700 years of the Holocene, Icelandic $U^{K'}_{37}$-SSTs decreased by nearly 1.5 °C from ~10.7 to ~10 kyrs BP, before levelling out at ~9 °C for the next 900 years. $\delta^{18}O$ analyses of foraminifera reveal that the IC started to influence the northern Denmark Strait 11 kyrs BP ago and was fully established by 10.2 kyrs BP (Ólafsdóttir et al., 2010). Reconstructed high marine paleoproductivity in Ísafjarðardjúp fjord during much of the early Holocene also points towards a penetration of nutrient rich Atlantic waters to the core site (Moossen et al., 2013). Despite the relatively warm Atlantic water transport of the IC, the occurrence of sea-ice indicating foraminifera and diatoms suggests that the Denmark Strait was also influenced by glacial melt water pulses, and/or repeated lateral shifts of the polar front (Andersen et al., 2004; Jennings et al., 2011). Benthic foraminiferal $\delta^{18}O$ analyses from Ísafjarðardjúp fjord indicate that the coring site was influenced by glacial melt water throughout the early Holocene (Quillmann et al., 2010). Such melt water pulses can be attributed to a second, regional, climate driving mechanism: the residual melting of northern hemisphere ice sheets following the last glacial maximum. After the glacial advance throughout the Younger Dryas, the main ice sheet covering the Icelandic Highlands was retreating at 10.3 kyr BP (Geirsdottir et al., 2009a), and the distal Greenland (Jennings et al., 2011), and Laurentide ice sheets (Alley and Ágústsdóttir, 2005) were also melting. Continual sea level rise suggests that land locked glaciers melted throughout the early, and into the middle Holocene until ~7 kyr BP (Siddall et al., 2010). Therefore, we attribute the dampened $U^{K'}_{37}$-SSTs, that are divergent from the CBT/MBT'-MAT trend and solar insolation, to the pervasive influence of glacial melt water in the early Holocene.

The early Holocene $U^{K'}_{37}$-SST record reveals two warm periods wherein SSTs rose by up to 2 °C, lasting from ~8.9 to ~8.5 kyrs BP and from ~8.1 to ~7.9 kyrs BP, that coincide with periods of high sunspot numbers (Solanki et al., 2004; Fig. 6f). Peak to peak comparison of these intervals reveals that cooler background climate between ~8.5 and ~7.9 kyrs BP may have been driven by generally low sunspot numbers, with SST peaks coeval with transient spikes in solar activity. A similarly long (8.7 to 7.9 kyr BP) cool period is also evident from two lacustrine sites in central and north Iceland (Geirsdóttir et al., 2013; Larsen et al., 2012). The link between low sunspot numbers and low $U^{K'}_{37}$-SSTs is supported by Rohling and Palike (2005), who hypothesise that proxies reconstructing summer climate are driven by the suns activity. Modern Icelandic coastal waters feature an insolation induced thermocline during the summer months, resulting in a sharp temperature gradient from warmer surface waters to cooler deeper waters (Hanna et al., 2006). It seems likely that the Ísafjarðardjúp fjord water column was similarly, if not more stratified during the early Holocene when high summer insolation and glacial melt water events occurred. This mechanism could explain the coherence noted above between solar activity and the $U^{K'}_{37}$-SST proxy. We note that there is no discernible relationship between $U^{K'}_{37}$-SSTs and sun spot numbers elsewhere in the early Holocene, possibly due to internal mechanisms, e.g. melt water events causing colder SSTs and masking the effect of increased solar activity on the $U^{K'}_{37}$-SSTs.

The hypothesis that $U^{K'}_{37}$-SSTs are likely biased towards summer season temperatures may also explain the lack of a notable $U^{K'}_{37}$-SST drop during the 8.2 event, since Rohling and Palike (2005) suggest that summer season proxies do not sensitively record the 8.2 event. In contrast to the $U^{K'}_{37}$-SSTs, the $\delta^{18}O$ record of benthic foraminifera from the same sediment core indicates a cooling and freshening of the IC at this time (Quillmann et al., 2012). Therefore, the biomarker and $\delta^{18}O$ proxy records reveal a possible decoupling of surface photic zone summer temperatures from deeper thermocline temperatures and increased stratification of the Denmark Strait water column during the early Holocene summer season.

All three precipitation records indicate that Iceland experienced a dryer than average summer climate during the early Holocene. Models indicate that the Icelandic low was located further north and stronger, than present, driving a stronger westerly jet, with increased precipitation and temperatures in winter (Harrison et al., 1992). The summer simulation of the same model suggests a reduced westerly jet during summer that would have led to a drier summer climate in north and central Europe (Harrison et al., 1992). Our precipitation proxies likely reflect summer, rather than winter precipitation (see discussion above), explaining their agreement with the modelled summer climate of the early Holocene. Not only the strength, but also the more northerly trajectory of the westerlies traversing the North Atlantic (Harrison et al., 1992; Knudsen et al., 2011) may have affected the precipitation regime. The proximity of the Greenland and Laurentide ice sheets may have contributed to the cooling of the westerlies causing them to hold less moisture and consequently resulting in a dryer Icelandic summer climate throughout the early Holocene. Finally, melt water induced cooling of regional SSTs may have contributed to lower precipitation: cold water evaporates less readily than warmer water, yielding relatively dryer maritime air masses, subsequently reduced precipitation on adjacent land masses.

The relatively high insolation and air temperatures coupled with the drier climate of the early Holocene would have caused relative increases in soil water evaporation and leaf water transpiration, leaving the available water for *n*-alkane biosynthesis depleted of the light isotope (Sachse et al., 2012). We argue that this depletion is reflected in the high δD_{C29} values measured during the early Holocene, compared to the average Holocene conditions (Fig. 6e).

Interestingly, our record indicates that leaf wax isotopic values dropped by nearly 10 ‰ at the onset of the 8.2 kyr event and then recovered afterwards. None of the other climate proxies (both temperature and precipitation) show a significant response to the 8.2 kyr event. Models suggest the catastrophic influx of glacial melt-waters resulted in isotopically depleted surface waters in the North Atlantic region for decades after the initial event, regardless of the isotopic effects of any synchronous changes in temperature and precipitation (LeGrande and Schmidt, 2008). Thus in our record the transient changes to more negative isotope values at 8.2 kyr BP (and perhaps at 8.7 kyr BP) may reflect changes in the δD of the precipitation source, rather than local climate impacts or a change in precipitation source/pathway.

4.2. Mid-Holocene and Neoglaciation (7.8 - 3.2 ka)

At the transition from the early to the middle Holocene, while summer insolation and CBT/MBT'-MAT decreased, two rapid $U^{K'}_{37}$-SST warming events occurred (Fig. 6a). Centred on 7.6 and 7.3 kyr BP, both events lasted ~300 years, during which $U^{K'}_{37}$-SSTs spiked by ~5 °C (rising by a remarkable 0.5 °C per decade). Following the second event SSTs rose steadily over the next 1400 years by ~4 °C. These $U^{K'}_{37}$-SST peaks coincide with Bond cycles 5 and 4 (Fig. 6g). We term the period between 7.8 and 5.5 kyrs BP the 'marine Holocene thermal maximum (HTM)' as the highest $U^{K'}_{37}$-SSTs are observed during this interval. The marine HTM broadly coincides with diatom and coccolithophore based evidence for increased Atlantic water penetration onto the northwest Icelandic Shelf (Giraudeau et al., 2010; Justwan et al., 2008) and the highest SSTs observed off of south east Greenland (Jennings et al., 2011) and the North Icelandic Shelf (Justwan et al., 2008; Fig. 6j) Furthermore, a major increase in reconstructed flow speed of the North Atlantic deep water across the Iceland-Scotland overflow ridge is centred on 7.2 kyr BP (Hall et al., 2004; Fig. 6k). As regional components of the AMOC, deep-water flow speeds across the Iceland-Scotland ridge and the northward flow of warm surface currents in the Nordic Seas (including the Denmark Strait) are thought to be linked (Hall et al., 2004; Renssen et al., 2005), suggesting increased AMOC velocity acting as a contributing driver for the high $U^{K'}_{37}$-SSTs of the marine HTM.

The cessation of glacial melt water events at the transition from the early to middle Holocene affords a complimentary explanation for the marine HTM. $\delta^{18}O$ signatures of *C. lobatulus* show that melt water pulses stopped affecting Ísafjarðardjúp waters from 7.9 kyr BP onwards (Quillmann et al., 2010). Intriguingly this coincides with the start of the first rapid $U^{K'}_{37}$-SST warming event noted above (Fig. 6a). This suggests that, once the dampening effect of glacial melt-water was removed, the still high (albeit decreasing) solar insolation, combined with a period of increased AMOC flow speed, drove a series of high SST episodes in Ísafjarðardjúp fjord.

The most striking observation when comparing the CBT/MBT'-MAT and $U^{K'}_{37}$-SST records is the temporal offset of ~3000 years between the maxima of the terrestrial HTM (~9.5 kyr BP) and the marine HTM (~6.5 kyr BP). Terrestrial and marine paleoclimate archives in the Iceland/Greenland region indicate that the HTM started at 8.6 ± 1.6 kyrs, and ended at 5.4 ± 1.4 kyrs (Kaufman et al., 2004). The uncertainties associated with the onset and end of the HTM may be due to the time it takes biologically based proxies to adjust to the HTM, i.e. the time it took *Betula* pollen to form mature vegetation and subsequently enough of a sedimentary pollen signature to be found in the paleoclimate record (Caseldine et al., 2003; Kaufman et al., 2004).

However, uncertainties in the timing of the HTM may also be due to the delayed response of specific parts of the environment to solar insolation as a climatic driver (Kaufman et al., 2004). One example is the spatial variability of the onset/termination of the HTM across the European/American Arctic sector. While the residual Laurentide ice sheet may have prevented the HTM from being expressed at sites surrounding the Hudson Bay, proxy records from Iceland were already influenced by the HTM (Kaufman et al., 2004).

In line with the latter explanation, we attribute the observed temporal discrepancy between the terrestrial and the marine HTM to the different responses of terrestrial and marine environments to solar radiation. Specifically, melt-water pulses dampened $U^{K'}_{37}$-SSTs during the early Holocene while CBT/MBT'-MATs were already driven by high insolation. Subsequently, $U^{K'}_{37}$-SSTs rose rapidly to form the marine HTM, ‘delayed’ by ~3000 years, but driven by declining, yet still high solar insolation, and possibly an accelerating AMOC.

We place the late Holocene neoglaciation between ~5.8 and ~3.2 kyrs BP, where both the $U^{K'}_{37}$-SST, and the CBT/MBT'-MAT records indicate decreasing temperatures in tandem with decreasing summer insolation. This corroborates observations from marine (Jennings et al., 2002; Justwan et al., 2008; Fig. 6j; Moros et al., 2006), and terrestrial records from Iceland (Geirsdóttir et al., 2013; Larsen et al., 2012; Moossen et al., 2013; Wastl et al., 2001). The neoglaciation culminated at ~3.2 kyrs BP with some of the lowest $U^{K'}_{37}$-SST and CBT/MBT'-MAT temperatures observed (Figs. 6a, b), coinciding with a global cool episode recognised in a number of records (Mayewski et al., 2004 and references therein). The late neoglacial decline in marine and terrestrial temperatures is clearly driven by declining insolation. However, an additional driver may have been the decelerating AMOC (contributing to the $U^{K'}_{37}$-SST decrease), culminating in the 2.7 ka event, as evidenced by declining Iceland Scotland overflow velocities (Hall et al., 2004; Fig. 6k).

The soil pH and $ACL_{25\text{-}35}$ precipitation proxies (and to a lesser degree the δD_{C29} proxy) show a transition from less than average, to more than average precipitation at the onset of the middle Holocene (Figs. 6c,d,e) through to its termination ~3.2 kyr BP ago. Increasing precipitation throughout the middle Holocene is consistent with increased windiness/storms in Iceland and Greenland (Jackson et al., 2005; O'Brien et al., 1995), and with increased winter precipitation in western Norway (Bjune et al., 2005). The precipitation maxima throughout the middle Holocene may be explained by the large scale atmospheric shifts associated with declining summer insolation during this period (Knudsen et al., 2011). Specifically, the declining summer insolation gradient between the high and low latitudes (Laskar et al., 2004), caused a southward displacement of the ITCZ (Haug et al., 2001), the westerly jet across the North Atlantic and the mean position of the Icelandic low (Harrison et al., 1992). Our new precipitation data corroborates the scenario of Knudsen et al. (2011) that indicates that Iceland was situated directly in the path of the southwardly displaced, moisture carrying westerlies throughout the middle Holocene, and experienced high precipitation (Figs. 6c,d,e).

A clear correlation between increased precipitation in Iceland and NAO+ periods, has been observed in the instrumental record (Hanna et al., 2004; Hurrell, 1995). Proxy reconstructions of NAO variability now extend back through the MCA (Trouet et al., 2009), to 5.2 kyrs BP (Olsen et al., 2012). If the contemporary link between increased precipitation and NAO+ periods holds true throughout the Holocene, then our precipitation records suggest that a persistent NAO+ atmospheric pattern was prevalent from at least 7.5 kyrs BP onwards, lasting until the end of the middle Holocene at 3.2 kyr BP. Evidence for increased storminess during the middle Holocene in Iceland (Jackson et al., 2005), along with a predominantly positive mode of the NAO, as reconstructed from Greenland lake redox states for much of the middle Holocene (Olsen et al., 2012) supports our hypothesis. Finally, the NAO may also have influenced North Atlantic SSTs during the middle Holocene (Andersen et al., 2004), however such variability is not obviously expressed in our $U^{K'}_{37}$-SST record.

4.3. Late Holocene climate variability and the evolution of the modern NAO (3.2 - 0.3 ka)

The late Holocene is the most socially relevant period in this study because of the clear and persistent influence climatic fluctuations had on human societies (Buntgen et al., 2011; D'Andrea et al., 2011; deMenocal, 2001). Our proxy records indicate that all climate parameters, precipitation, air-, and sea surface temperature underwent noteworthy change at the transition from the middle to the late Holocene (Figs. 6 and 7a, b, c, d, e).

From ~3.2 kyrs BP, the reconstructed CBT/MBT'-MAT and $U^{K'}_{37}$-SST temperature trends deviate from the continually decreasing summer insolation (Figs 6a, b). Intriguingly, the late Holocene is the only period where the CBT/MBT'-MAT reconstruction does not follow insolation change. The simultaneous decoupling of both CBT/MBT'-MAT and $U^{K'}_{37}$-SST records from insolation indicates a threshold, after which, a driving mechanism other than insolation started to dominate air and sea surface temperature variations over the most recent ~3.2 kyrs BP. Along with the temperature records, the soil pH precipitation record indicates a gradual, while the ACL_{25-35} and dD_{C29} records show a more abrupt precipitation decrease (Figs 6 and 7c, d, e). The periods from ~2.2 to ~1.3 kyrs BP, and from ~1.1 to ~0.5 kyrs BP are characterised by relatively warm $U^{K'}_{37}$-SSTs, while CBT/MBT'-MATs tend to be cool, and precipitation tends to be elevated. Within ^{14}C-AMS dating errors, these periods coincide with the Roman Warm Period (RWP), and the MCA (Geirsdóttir et al., 2013; Graham et al., 2011). In comparison, the periods from ~1.3 to ~1.1 kyrs BP, and from ~0.5 kyrs BP to ~0.3 kyrs BP, are characterised by cooler $U^{K'}_{37}$-SSTs, warmer CBT/MBT'MATs, and lower precipitation. These periods coincide with the Dark Ages (DA; also known as the migration period; Buntgen et al., 2011; Sicre et al., 2008a) and the onset of the LIA (Ogilvie and Jonsson, 2001). In contrast with the asynchronous trends of precipitation, marine and terrestrial temperatures during the middle and early Holocene, all climate proxy records exhibit changes over four distinct climatic periods covering most of the late Holocene. This suggests one dominant controlling mechanism, most plausibly the NAO, which is known to affect sea surface temperature, air temperature and precipitation in Northern Europe and the North Atlantic sector (Hurrell, 1995; Hurrell et al., 2003). Assuming that the relationship between contemporary instrumental observations of precipitation, sea surface-, and air temperatures, and the NAO have remained constant throughout the late Holocene we would expect to observe the following climatic variations during positive NAO phases (compared to negative NAO phases): higher precipitation over Iceland (Hurrell, 1995; Hurrell et al., 2003; Figs. 1c, d), a higher throughput of warm Atlantic waters through the Denmark Strait, and therefore warmer SSTs (Blindheim and Malmberg, 2005; Figs. 1e, f). Higher air temperatures might also be expected, however, the link between air temperature and NAO is tenuous on Iceland (Hanna et al., 2004; Ólafsdóttir et al., 2013). The variability of the $U^{K'}_{37}$-SSTs and the precipitation records throughout the MCA and the LIA is in good agreement with reconstructed NAO variability (Olsen et al., 2012; Trouet et al., 2009; Figs. 6h, i and 7f, g), lending credence to our hypothesis that NAO was the dominant forcing mechanism of Icelandic climate throughout the late Holocene.

Interestingly, Late Holocene centennial-scale CBT/MBT'-MAT variations are anti-phased with $U^{K'}_{37}$-SST throughout the RWP, DA, MCA and LIA (Figs. 6 and 7a, b). This would seemingly oppose contemporary (Hanna et al., 2004; Hurrell et al., 2003), and proxy based observations (Ólafsdóttir et al., 2013), of warmer air temperatures during NAO+ phases compared to NAO- phases. Specifically, the CBT/MBT'-MAT record indicates relatively low temperatures during the RWP and MCA (NAO+), compared to the higher reconstructed temperatures during the DA and LIA (NAO-). Additionally, the reconstructed CBT/MBT'-MAT temperatures are higher than the chironomid based August temperature reconstructed by Axford et al. (2009) during the DA and LIA, while the temperature records are in better agreement during the RWP and MCA. This suggests, that Icelandic CBT/MBT'-MAT temperature reconstructions provide temperature estimates that are too high during the periods characterised by NAO- periods. We hypothesise that this counterintuitive relationship between reconstructed CBT/MBT'-MAT and NAO mode is due to the proxies molecular variations that are mediated by soil bacteria, making the proxy a first order recorder of soil temperature change (Weijers et al., 2007b). Contemporary observations show that negative precipitation anomalies cause increased summer warmth throughout central Europe and are correlated to NAO fluctuations due to decreased latent cooling from soil moisture (Wang et al., 2011). Furthermore, dry soils warm more readily than wet soils (Al-Kayssi et al., 1990). Thus we hypothesise that during NAO- periods (LIA, DA), while precipitation was low (Fig. 6 and 7c, d, e), surface soils became relatively dry and were warmed more easily by solar radiation, compared to the relatively wet soils of NAO+ periods (MCA, RWP). Consequently, the counterintuitive centennial scale CBT/MBT'-

MAT trends during the Late Holocene may indicate soil temperature variations as a result of predominantly dry vs. predominantly wet soil conditions during the late Holocene. Following this hypothesis, the CBT/MBT'-MAT proxy may indirectly provide information on NAO variability via temperature dependency of the soil on changing precipitation regimes. This is supported by the correlated CBT/MBT'-MAT and precipitation records, demonstrating the advantage of considering multiple independent biomarker records in concert.

The argument, that all proxy records shown here are mainly affected by NAO fluctuations during the late Holocene, is supported by REDFIT spectral analyses conducted on the $U^{K'}_{37}$-SST, CBT/MBT'-MAT, soil pH, and the ACL_{25-35}-proxy records (Schulz and Mudelsee, 2002; Fig. 8). We note that the sampling resolution between ~2.1 and ~7.3 kyrs BP is not high enough to resolve the high frequency periodicities observed in the spectral analyses (SI 1). Therefore we limit the following interpretation to the late Holocene, from ~2.1 to ~0.3 kyrs BP where the sample resolution is 25 years/sample. All four records reveal periodicities between 64 and 96 years at the 95% significance level (Fig. 8). Such periodicities in instrumental records have been associated with the NAO (Rossi et al., 2011). Moreover, these periodicities have also been observed in the NAO reconstructions from Greenland lakes (Olsen et al., 2012), and in a varve-thickness record from Iceland (Ólafsdóttir et al., 2013). We note that the $U^{K'}_{37}$-SST and the CBT/MBT'-MAT temperature reconstructions also exhibit a significant spectral peak at ~130 years which, along with the spectral peaks between 64 and 96 years is associated with the Atlantic Meridional Oscillation (AMO; Knudsen et al., 2011; Rossi et al., 2011), that describes oscillatory variability of North Atlantic SSTs (Kerr, 2000; Schlesinger and Ramankutty, 1994). The influence of the AMO has also been postulated in the varve-thickness record from Iceland (Ólafsdóttir et al., 2013).

Therefore it is plausible that the AMO, alongside the NAO played a role in the late Holocene climate variations.

As discussed above, our biomarker proxies from MD99-2266 are likely weighted towards a spring/summer signal, rather than mean annual climate variability. However, the NAO is most prevalent during winter months (Hurrell, 1995; Hurrell and Deser, 2009). Thus we need to reconcile how biomarker proxies reconstructing summer climate can detect an atmospheric signal that is most prevalent during winter months. Hurrell and Deser (2009; and references therein) show that winter NAO indices can affect the climate of the following year by affecting slower components of the climate system (e.g. oceanic currents). Wang et al. (2011) show that European summer temperatures are highly correlated with the NAO regime of the previous year. Regionally, Blindheim and Malmberg (2005) have shown that changes of the winter sea level pressure gradients across the Denmark Strait are significantly correlated with SSTs of the following spring. Based on these observations in the instrumental record it seems plausible that the biomarker records presented here are influenced by changing NAO regimes, particularly when one considers that the sediment analysed for each data point throughout the late Holocene integrates between 10 and 25 years of climate.

We suggest insolation ceased to be a dominant driver of centennial scale climate events at the turn from the middle to the late Holocene. Instead, during this period of relatively low insolation, the climatic influence of internal feedback mechanisms, namely the NAO (and possibly the AMO) increasingly drove centennial scale changes, which are superimposed on the longer term, monotonic, insolation driven change. This suggests that lateral energy transport via warm surface currents and south-westerly winds became more important for Icelandic climate, rather than continually decreasing insolation. This conclusion is supported by a varve thickness record from lake Hvítárvatn which indicates, that the NAO exerted increasing influence on Icelandic climate throughout the late Holocene (Ólafsdóttir et al., 2013).

5. Conclusions

The high-resolution, multi-proxy approach to climate reconstruction that is presented in this study gives a comprehensive picture of terrestrial and marine climate evolution throughout the Holocene. We show that major reorganisations of Holocene climate in Iceland took place at two climatic thresholds, one at ~7.8, and the other at ~3.2 kyrs BP. Based on the apparent changing importance of different climate drivers at ~7.3 and ~3.2 kyrs BP, we divide the Holocene into three distinct climatic periods, the early, middle and late Holocene. These climatic threshold events only become evident when considering the high-resolution terrestrial and marine biomarker proxy data in concert, illustrating the importance of the multi-proxy approach adopted here.

The combination of multiple biomarker proxies increases overall confidence in our interpretations and also reveals strengths and weaknesses of a particular proxy. For example, the confidence we have in the interpretation of soil pH, $ACL_{25\text{-}35}$, and δD_{C29} as recorders of precipitation is increased by the fact that all three records are in good agreement. Furthermore, the multi-proxy approach also reveals that the CBT/MBT'-MAT record may be significantly influenced by precipitation along with air temperature. The counterintuitive behaviour of the CBT/MBT'-MAT record in the late Holocene can be explained if the precipitation proxies are considered.

CBT/MBT'-MATs were mainly driven by high insolation causing the terrestrial HTM throughout the early Holocene (10.7 - 7.8 kyrs BP). In contrast, $U^{K'}_{37}$-SSTs appear to be dampened by the pervasive influence of glacial melt water events. Furthermore, the centennial variability in the $U^{K'}_{37}$-SST record illustrates the influence of solar activity, superimposed on the millennial scale melt water influence. The precipitation records indicate a dryer than average early Holocene summer climate, driven by: a reduced westerly jet during the summer months (Harrison et al., 1992) and reduced evaporation in source waters, due to the pervasive influence of melt water events.

The influence of melt water on the $U^{K'}_{37}$-SST record ceases at the transition of the early to the middle Holocene. Subsequently, an accelerating AMOC and decreasing, yet still high insolation drove a strong marine HTM that occurred ~3 kyrs after its terrestrial equivalent. The neoglacial period dominated the latter part of the middle Holocene and was driven by continually decreasing insolation, although the decelerating AMOC likely also affected $U^{K'}_{37}$-SSTs. Precipitation increased and remained high throughout the middle Holocene. The transition from a dryer to wetter than average climate is attributed to a decreasing summer insolation gradient that caused a southward shift of oceanic (AMO) and atmospheric (Iceland low and westerlies jet) circulation systems (Harrison et al., 1992; Knudsen et al., 2011). This shift placed Iceland under the direct influence of moisture carrying westerlies and drove the high precipitation regime of the middle Holocene.

All the paleoclimate records exhibit synchronous variability across four distinct climatic periods, the RWP, DA, MCA and LIA in the late Holocene. The comparison between of the precipitation, $U^{K'}_{37}$-SST and CBT/MBT'-MAT datasets presented here, and the NAO reconstructions by Trouet et al. (2009) and Olsen et al. (2012) indicates that the NAO became the dominant driver of Icelandic climate throughout the late Holocene. Furthermore, In conjunction with the NAO reconstruction of Olsen et al.

(2012), our data demonstrates that the observed link between increased precipitation in Iceland during NAO+ phases (Hurrell, 1995), that has previously been extended to the beginning of the MCA (Trouet et al., 2009), may have existed nearly from the onset of the middle Holocene at ~7.5 kyrs BP. Furthermore, assuming that NAO-type atmospheric fluctuations are the primary driver of high precipitation throughout the whole of the middle Holocene, our data indicates that the NAO was predominantly in a positive mode from ~ 7.8 to ~3.2 kyrs BP. If the amount of precipitation can be correlated with the strength of the westerlies ("strength" of the NAO), then our precipitation data shows that the westerlies (and possibly the NAO) were considerably stronger during the middle Holocene, compared to the late Holocene.

This study demonstrates that the interaction of different climate drivers drove the complex Holocene climate history. It agrees with findings of Larsen et al. (2012) and Geirsdóttir et al. (2013) who attribute the non-linear response of their palaeoclimate reconstructions to insolation to regional and local climate feedback mechanisms. In light of the fact that different climate drivers have shaped Icelandic climate throughout the early, middle and late Holocene, trying to ascribe pervasive climatic cycles spanning the entire Holocene (i.e. Bond cycles) to a single forcing mechanism would seemingly be futile. This conclusion offers one explanation as to why so many researchers have not been able to identify all, or even any Bond cycles in their Holocene records (Wanner et al., 2011).

6. Acknowledgements

We thank an anonymous reviewer for the helpful and insightful comments. We thank the crew and staff of the *Marion Dufresne II*, and the CALYPSO coring team on the 1999 IMAGES cruise. We also thank Professor John Andrews for providing the core material for this research, and the technical staff at the Institute of Arctic and Alpine Research. We thank Dr. Richard Pancost and technical staff at the Organic Geochemistry Unit, Bristol. We thank Dr. Ellen Roosen from the Woods Hole Oceanographic Institution who sent additional u-channels of the top most 3.5 meters of the sediment core archive half. We thank Dr. Fiona Meade for her help on Fig. 1 (https://sites.google.com/site/meadescientificservices). We thank the Scottish Alliance for Geoscience, Environment and Society (SAGES) who funded the PhD to Dr. Heiko Moossen. We thank the Japanese society for the promotion of science (JSPS) for funding a two months bursary to Dr. Heiko Moossen to Hokkaido University.

7. References

Al-Kayssi, A.W., Al-Karaghouli, A.A., Hasson, A.M., Beker, S.A., 1990. Influence of Soil Moisture Content on Soil Temperature and Heat Storage under Greenhouse Conditions. Journal of Agricultural Engineering Research 45, 241-252.

Alley, R.B., Ágústsdóttir, A.M., 2005. The 8k event: cause and consequences of a major Holocene abrupt climate change. Quaternary Science Reviews 24, 1123-1149.

Andersen, C., Koc, N., Jennings, A., Andrews, J.T., 2004. Nonuniform response of the major surface currents in the Nordic Seas to insolation forcing: Implications for the Holocene climate variability. Paleoceanography 19.

Andrews, J.T., Harðardóttir, J., Stoner, J.S., Principato, S.M., 2008. Holocene sediment magnetic properties along a transect from Isafiardardiup to Djupall, Northwest Iceland. Arctic Antarctic and Alpine Research 40, 1-14.

Andrews, J.T., Jennings, A.E., 2014. Multidecadal to millennial marine climate oscillations across the Denmark Strait (similar to 66 degrees N) over the last 2000 cal yr BP. Climate of the Past 10, 325-343.

Arnalds, O., 2008. Soils of Iceland. Jokull 58, 409-421.

Axford, Y., Andresen, C.S., Andrews, J.T., Belt, S.T., Geirsdóttir, Á., Massé, G., Miller, G.H., Ólafsdóttir, S., Vare, L.L., 2011. Do paleoclimate proxies agree? A test comparing 19 late Holocene climate and sea-ice reconstructions from Icelandic marine and lake sediments. Journal of Quaternary Science 26, 645-656.

Axford, Y., Geirsdóttir, Á., Miller, G., Langdon, P., 2009. Climate of the Little Ice Age and the past 2000 years in northeast Iceland inferred from chironomids and other lake sediment proxies. Journal of Paleolimnology 41, 7-24.

Badewien, T., Vogts, A., Dupont, L., Rullkötter, J., 2015. Influence of Late Pleistocene and Holocene climate on vegetation distributions in southwest Africa elucidated from sedimentary n-alkanes – Differences between 12°S and 20°S. Quaternary Science Reviews 125, 160-171.

Bendle, J., Kawamura, K., Yamazaki, K., Niwai, T., 2007. Latitudinal distribution of terrestrial lipid biomarkers and *n*-alkane compound-specific stable carbon isotope ratios in the atmosphere over the western Pacific and Southern Ocean. Geochimica Et Cosmochimica Acta 71, 5934-5955.

Bendle, J., Rosell-Melé, A., 2004. Distributions of U^{K}_{37} and $U^{K'}_{37}$ in the surface waters and sediments of the Nordic Seas: Implications for paleoceanography. Geochemistry Geophysics Geosystems 5.

Bendle, J.A.P., Rosell-Melé, A., 2007. High-resolution alkenone sea surface temperature variability on the North Icelandic Shelf: implications for Nordic Seas palaeoclimatic development during the Holocene. The Holocene 17, 9-24.

Bjune, A.E., Bakke, J., Nesje, A., Birks, H.J.B., 2005. Holocene mean July temperature and winter precipitation in western Norway inferred from palynological and glaciological lake-sediment proxies. The Holocene 15, 177-189.

Blindheim, J., Malmberg, S.-A., 2005. The Mean Sea Level Pressure Gradient Across the Denmark Strait as an Indicator of Conditions in the North Icelandic Irminger Current, In: Drange, H., Dokkken, T., Furevik, T., Gerdes, R., Berger, W. (Eds.), The Nordic Seas: An Integrated Perspective. AGU, pp. 65-71.

Bond, G., Kromer, B., Beer, J., Muscheler, R., Evans, M.N., Showers, W., Hoffmann, S., Lotti-Bond, R., Hajdas, I., Bonani, G., 2001. Persistent solar influence on North Atlantic climate during the Holocene. Science 294, 2130-2136.

Bond, G., Showers, W., Cheseby, M., Lotti, R., Almasi, P., deMenocal, P., Priore, P., Cullen, H., Hajdas, I., Bonani, G., 1997. A pervasive millennial-scale cycle in North Atlantic Holocene and glacial climates. Science 278, 1257-1266.

Brassell, S.C., Eglinton, G., Marlowe, I.T., Pflaumann, U., Sarnthein, M., 1986. Molecular Stratigraphy - A new tool for climatic assessment. Nature 320, 129-133.

Broecker, W.S., 1997. Thermohaline Circulation, the Achilles Heel of Our Climate System: Will Man-Made CO2 Upset the Current Balance? Science 278, 1582-1588.

Buntgen, U., Tegel, W., Nicolussi, K., McCormick, M., Frank, D., Trouet, V., Kaplan, J.O., Herzig, F., Heussner, K.U., Wanner, H., Luterbacher, J., Esper, J., 2011. 2500 Years of European Climate Variability and Human Susceptibility. Science 331, 578-582.

Calvo, E., Pelejero, C., Logan, G.A., De Deckker, P., 2004. Dust-induced changes in phytoplankton composition in the Tasman Sea during the last four glacial cycles. Paleoceanography 19, 10.

Caseldine, C., Geirsdottir, A., Langdon, P., 2003. Efstadalsvatn - a multi-proxy study of a Holocene lacustrine sequence from NW Iceland. Journal of Paleolimnology 30, 55-73.

Castañeda, I.S., Schouten, S., 2011. A review of molecular organic proxies for examining modern and ancient lacustrine environments. Quaternary Science Reviews 30, 2851-2891.

Collins, J.A., Schefuß, E., Mulitza, S., Prange, M., Werner, M., Tharammal, T., Paul, A., Wefer, G., 2013. Estimating the hydrogen isotopic composition of past precipitation using leaf-waxes from western Africa. Quaternary Science Reviews 65, 88-101.

Conte, M.H., Sicre, M.A., Rühlemann, C., Weber, J.C., Schulte, S., Schulz-Bull, D., Blanz, T., 2006. Global temperature calibration of the alkenone unsaturation index ($U^{K'37}$) in surface waters and comparison with surface sediments. Geochemistry Geophysics Geosystems 7.

Craig, H., 1961. Isotopic Variations in Meteoric Waters. Science 133, 1702-1703.

D'Andrea, W.J., Huang, Y., Fritz, S.C., Anderson, N.J., 2011. Abrupt Holocene climate change as an important factor for human migration in West Greenland. Proceedings of the National Academy of Sciences of the United States of America 108, 9765-9769.

deMenocal, P.B., 2001. Cultural responses to climate change during the Late Holocene. Science 292, 667-673.

Eglinton, G., Gonzalez, A.G., Hamilton, R.J., Raphael, R.A., 1962. Hydrocarbon constituents of the wax coatings of plant leaves: a taxonomic survey. Phytochemistry 1, 89 - 102.

Eglinton, T.I., Eglinton, G., 2008. Molecular proxies for paleoclimatology. Earth and Planetary Science Letters 275, 1-16.

Fawcett, P.J., Werne, J.P., Anderson, R.S., Heikoop, J.M., Brown, E.T., Berke, M.A., Smith, S.J., Goff, F., Donohoo-Hurley, L., Cisneros-Dozal, L.M., Schouten, S., Sinninghe Damste, J.S., Huang, Y., Toney, J., Fessenden, J., WoldeGabriel, G., Atudorei, V., Geissman, J.W., Allen, C.D., 2011. Extended megadroughts in the southwestern United States during Pleistocene interglacials. Nature 470, 518-521.

Fietz, S., Huguet, C., Bendle, J., Escala, M., Gallacher, C., Herfort, L., Jamieson, R., Martinez-Garcia, A., McClymont, E.L., Peck, V.L., Prahl, F.G., Rossi, S., Rueda, G., Sanson-Barrera, A., Rosell-Mele, A., 2012. Co-variation of crenarchaeol and branched GDGTs in globally-distributed marine and freshwater sedimentary archives. Global and Planetary Change 92-93, 275-285.

Gao, L., Nie, J., Clemens, S., Liu, W., Sun, J., Zech, R., Huang, Y., 2012. The importance of solar insolation on the temperature variations for the past 110 kyr on the Chinese Loess Plateau. Palaeogeography, Palaeoclimatology, Palaeoecology 317–318, 128-133.

Geirsdottir, A., Andrews, J.T., Olafsdottir, S., Helgadottir, G., Hardardottir, J., 2002. A 36 Ky record of iceberg rafting and sedimentation from north-west Iceland. Polar Research 21, 291-298.

Geirsdottir, A., Miller, G.H., Axford, Y., Olafsdottir, S., 2009a. Holocene and latest Pleistocene climate and glacier fluctuations in Iceland. Quaternary Science Reviews 28, 2107-2118.

Geirsdóttir, Á., Miller, G.H., Larsen, D.J., Ólafsdóttir, S., 2013. Abrupt Holocene climate transitions in the northern North Atlantic region recorded by synchronized lacustrine records in Iceland. Quaternary Science Reviews 70, 48-62.

Geirsdottir, A., Miller, G.H., Thordarson, T., Olafsdottir, K.B., 2009b. A 2000 year record of climate variations reconstructed from Haukadalsvatn, West Iceland. Journal of Paleolimnology 41, 95-115.

Giraudeau, J., Grelaud, M., Solignac, S., Andrews, J.T., Moros, M., Jansen, E., 2010. Millennial-scale variability in Atlantic water advection to the Nordic Seas derived from Holocene coccolith concentration records. Quaternary Science Reviews 29, 1276-1287.

Graham, N.E., Ammann, C.M., Fleitmann, D., Cobb, K.M., Luterbacher, J., 2011. Support for global climate reorganization during the "Medieval Climate Anomaly". Clim Dyn 37, 1217-1245.

Gray, L.J., Beer, J., Geller, M., Haigh, J.D., Lockwood, M., Matthes, K., Cubasch, U., Fleitmann, D., Harrison, G., Hood, L., Luterbacher, J., Meehl, G.A., Shindell, D., van Geel, B., White, W., 2010. Solar influences on climate. Rev. Geophys. 48, 53.

Gronvold, K., Oskarsson, N., Johnsen, S.J., Clausen, H.B., Hammer, C.U., Bond, G., Bard, E., 1995. Ash layers from iceland in the Greenland GRIP ice core correlated with oceanic and land sediments. Earth and Planetary Science Letters 135, 149-155.

Grootes, P.M., Stuiver, M., 1997. Oxygen 18/16 variability in Greenland snow and ice with 10^{-3}-10^{-5} year time resolution. J. Geophys. Res. 102, 26455-26470.

Hall, I.R., Bianchi, G.G., Evans, J.R., 2004. Centennial to millennial scale Holocene climate-deep water linkage in the North Atlantic. Quaternary Science Reviews 23, 1529-1536.

Hallsdottir, M., 1995. On the pre-settlement history of Icelandic vegetation. Buvisindi 9, 17-29.

Hammer, Ø., Harper, D.A.T., Ryan, P.D., 2001. PAST: Paleontoogical Statistics software package for education and data analysis. Palaeontologia Electroniac 4(1):9 pp., 2.17c ed.

Hanna, E., Jonsson, T., Box, J.E., 2004. An analysis of Icelandic climate since the nineteenth century. International Journal of Climatology 24, 1193-1210.

Hanna, E., Jonsson, T., Olafsson, J., Valdimarsson, H., 2006. Icelandic coastal sea surface temperature records constructed: Putting the pulse on air-sea-climate interactions in the northern North Atlantic. Part I: Comparison with HadISST1 open-ocean surface temperatures and preliminary analysis of long-term patterns and anomalies of SSTs around Iceland. Journal of Climate 19, 5652-5666.

Hansen, B., Østerhus, S., 2000. North Atlantic-Nordic Seas exchanges. Progress In Oceanography 45, 109-208.

Harrison, S.P., Prentice, I.C., Bartlein, P.J., 1992. Influence of insolation and glaciation on atmospheric circulation in the North Atlantic sector: Implications of general circulation model experiments for the Late Quaternary climatology of Europe. Quaternary Science Reviews 11, 283-299.

Haug, G.H., Hughen, K.A., Sigman, D.M., Peterson, L.C., Röhl, U., 2001. Southward Migration of the Intertropical Convergence Zone through the Holocene. Science 293, 1304-1308.

Hopmans, E.C., Weijers, J.W.H., Schefuss, E., Herfort, L., Damste, J.S.S., Schouten, S., 2004. A novel proxy for terrestrial organic matter in sediments based on branched and isoprenoid tetraether lipids. Earth and Planetary Science Letters 224, 107-116.

Howe, J.A., Austin, W.E.N., Forwick, M., Paetzel, M., Harland, R., Cage, A.G., 2010. Fjord systems and archives: a review. Geological Society, London, Special Publications 344, 5-15.

Hurrell, J.W., 1995. Decadal trends in the North Atlantic Oscillation - Regional temperatures and precipitation. Science 269, 676-679.

Hurrell, J.W., Deser, C., 2009. North Atlantic climate variability: The role of the North Atlantic Oscillation. Journal of Marine Systems 78, 28-41.

Hurrell, J.W., Kushiner, Y., Ottersen, G., Visbeck, M., 2003. An overview of the North Atlantic Oscillation. American Geophysical Union, Washington, DC, ETATS-UNIS.

Ineson, S., Scaife, A.A., Knight, J.R., Manners, J.C., Dunstone, N.J., Gray, L.J., Haigh, J.D., 2011. Solar forcing of winter climate variability in the Northern Hemisphere. Nature Geosci 4, 753-757.

Jackson, M.G., Oskarsson, N., Trønnes, R.G., McManus, J.F., Oppo, D.W., Grönvold, K., Hart, S.R., Sachs, J.P., 2005. Holocene loess deposition in Iceland: Evidence for millennial-scale atmosphere-ocean coupling in the North Atlantic. Geology 33, 509-512.

Jennings, A., Andrews, J., Wilson, L., 2011. Holocene environmental evolution of the SE Greenland Shelf North and South of the Denmark Strait: Irminger and East Greenland current interactions. Quaternary Science Reviews 30, 980-998.

Jennings, A.E., Knudsen, K.L., Hald, M., Hansen, C.V., Andrews, J.T., 2002. A mid-Holocene shift in Arctic sea-ice variability on the East Greenland Shelf. Holocene 12, 49-58.

Johnson, D.W., Hanson, P.J., Todd, D.E., Susfalk, R.B., Trettin, C.F., 1998. Precipitation Change and Soil Leaching: Field Results and Simulations from Walker Branch Watershed, Tennessee. Water, Air, & Soil Pollution 105, 251-262.

Justwan, A., Koç, N., Jennings, A.E., 2008. Evolution of the Irminger and East Icelandic Current systems through the Holocene, revealed by diatom-based sea surface temperature reconstructions. Quaternary Science Reviews 27, 1571-1582.

Kaufman, D.S., Ager, T.A., Anderson, N.J., Anderson, P.M., Andrews, J.T., Bartlein, P.J., Brubaker, L.B., Coats, L.L., Cwynar, L.C., Duvall, M.L., Dyke, A.S., Edwards, M.E., Eisner, W.R., Gajewski, K., Geirsdóttir, A., Hu, F.S., Jennings, A.E., Kaplan, M.R., Kerwin, M.W., Lozhkin, A.V., MacDonald, G.M., Miller, G.H., Mock, C.J., Oswald, W.W., Otto-Bliesner, B.L., Porinchu, D.F., Rühland, K., Smol, J.P., Steig, E.J., Wolfe, B.B., 2004. Holocene thermal maximum in the western Arctic (0-180°W). Quaternary Science Reviews 23, 529-560.

Kawamura, K., Ishimura, Y., Yamazaki, K., 2003. Four years' observations of terrestrial lipid class compounds in marine aerosols from the western North Pacific. Global Biogeochem. Cycles 17, 1003.

Kerr, R.A., 2000. A North Atlantic climate pacemaker for the centuries. Science 288, 1984-1986.

Knudsen, M.F., Seidenkrantz, M.-S., Jacobsen, B.H., Kuijpers, A., 2011. Tracking the Atlantic Multidecadal Oscillation through the last 8,000 years. Nature Communications 2.

Langdon, P.G., Leng, M.J., Holmes, N., Caseldine, C.J., 2010. Lacustrine evidence of early-Holocene environmental change in northern Iceland: a multiproxy palaeoecology and stable isotope study. Holocene 20, 205-214.

Larsen, D.J., Miller, G.H., Geirsdóttir, Á., Ólafsdóttir, S., 2012. Non-linear Holocene climate evolution in the North Atlantic: a high-resolution, multi-proxy record of glacier activity and environmental change from Hvítárvatn, central Iceland. Quaternary Science Reviews 39, 14-25.

Laskar, J., Robutel, P., Joutel, F., Gastineau, M., Correia, A.C.M., Levrard, B., 2004. A long-term numerical solution for the insolation quantities of the Earth. Astronomy & Astrophysics 428, 261-285.

LeGrande, A.N., Schmidt, G.A., 2008. Ensemble, water isotope-enabled, coupled general circulation modeling insights into the 8.2 ka event. Paleoceanography 23.

Mayewski, P.A., Rohling, E.E., Stager, J.C., Karlen, W., Maasch, K.A., Meeker, L.D., Meyerson, E.A., Gasse, F., van Kreveld, S., Holmgren, K., Lee-Thorp, J., Rosqvist, G., Rack, F., Staubwasser, M., Schneider, R.R., Steig, E.J., 2004. Holocene climate variability. Quaternary Research 62, 243-255.

Moossen, H., Abell, R., Quillmann, U., Bendle, J., 2013. Holocene changes in marine productivity and terrestrial organic carbon inputs into an Icelandic fjord: Application of molecular and bulk organic proxies. The Holocene 23, 11.

Moros, M., Andrews, J.T., Eberl, D.D., Jansen, E., 2006. Holocene history of drift ice in the northern North Atlantic: Evidence for different spatial and temporal modes. Paleoceanography 21, PA2017.

Niedermeyer, E.M., Schefuß, E., Sessions, A.L., Mulitza, S., Mollenhauer, G., Schulz, M., Wefer, G., 2010. Orbital- and millennial-scale changes in the hydrologic cycle and vegetation in the western African Sahel: insights from individual plant wax δD and $\delta^{13}C$. Quaternary Science Reviews 29, 2996-3005.

O'Brien, S.R., Mayewski, P.A., Meeker, L.D., Meese, D.A., Twickler, M.S., Whitlow, S.I., 1995. Complexity of Holocene climate as reconstructed from a Greendland ice core. Science 270, 1962-1964.

Ogilvie, A.E.J., Jonsson, T., 2001. "Little Ice Age" research: A perspective from Iceland. Climatic Change 48, 9-52.

Ólafsdóttir, K.B., Geirsdóttir, Á., Miller, G.H., Larsen, D.J., 2013. Evolution of NAO and AMO strength and cyclicity derived from a 3-ka varve-thickness record from Iceland. Quaternary Science Reviews 69, 142-154.

Ólafsdóttir, S., Jennings, A.E., Geirsdóttir, Á., Andrews, J., Miller, G.H., 2010. Holocene variability of the North Atlantic Irminger current on the south- and northwest shelf of Iceland. Marine Micropaleontology 77, 101-118.

Olsen, J., Anderson, N.J., Knudsen, M.F., 2012. Variability of the North Atlantic Oscillation over the past 5,200 years. Nature Geoscience 5, 808-812.

Peterse, F., Kim, J.-H., Schouten, S., Kristensen, D.K., Koç, N., Sinninghe Damsté, J.S., 2009. Constraints on the application of the MBT/CBT palaeothermometer at high latitude environments (Svalbard, Norway). Organic Geochemistry 40, 692-699.

Peterse, F., Nicol, G.W., Schouten, S., Sinninghe Damsté, J.S., 2010. Influence of soil pH on the abundance and distribution of core and intact polar lipid-derived branched GDGTs in soil. Organic Geochemistry 41, 1171-1175.

Peterse, F., van der Meer, J., Schouten, S., Weijers, J.W.H., Fierer, N., Jackson, R.B., Kim, J.-H., Sinninghe Damsté, J.S., 2012. Revised calibration of the MBT–CBT paleotemperature proxy based on branched tetraether membrane lipids in surface soils. Geochimica et Cosmochimica Acta 96, 215-229.

Prahl, F.G., Rontani, J.F., Zabeti, N., Walinsky, S.E., Sparrow, M.A., 2010. Systematic pattern in $U^{K'37}$ Temperature residuals for surface sediments from high latitude and other oceanographic settings. Geochimica Et Cosmochimica Acta 74, 131-143.

Prahl, F.G., Wakeham, S.G., 1987. Calibration of unsaturation patterns in long-chain ketone compositions for paleotemperature assessment. Nature 330, 367-369.

Quillmann, U., Jennings, A., Andrews, J., 2010. Reconstructing Holocene palaeoclimate and palaeoceanography in Isafjaroardjup, northwest Iceland, from two fjord records overprinted by relative sea-level and local hydrographic changes. Journal of Quaternary Science 25, 1144-1159.

Quillmann, U., Marchitto, T.M., Jennings, A.E., Andrews, J.T., Friestad, B.F., 2012. Cooling and freshening at 8.2 ka on the NW Iceland Shelf recorded in paired $\delta^{18}O$ and Mg/Ca measurements of the benthic foraminifer *Cibicides lobatulus*. Quaternary Research 78, 528-539.

Renssen, H., Goosse, H., Fichefet, T., Brovkin, V., Driesschaert, E., Wolk, F., 2005. Simulating the Holocene climate evolution at northern high latitudes using a coupled atmosphere-sea ice-ocean-vegetation model. Clim Dyn 24, 23-43.

Rohling, E.J., Palike, H., 2005. Centennial-scale climate cooling with a sudden cold event around 8,200 years ago. Nature 434, 975-979.

Rommerskirchen, F., Eglinton, G., Dupont, L., Rullkötter, J., 2006a. Glacial/interglacial changes in southern Africa: Compound-specific δ13C land plant biomarker and pollen records from southeast Atlantic continental margin sediments. Geochemistry, Geophysics, Geosystems 7, Q08010.

Rommerskirchen, F., Plader, A., Eglinton, G., Chikaraishi, Y., Rullkötter, J., 2006b. Chemotaxonomic significance of distribution and stable carbon isotopic composition of long-chain alkanes and alkan-1-ols in C4 grass waxes. Organic Geochemistry 37, 1303-1332.

Rossi, A., Massei, N., Laignel, B., 2011. A synthesis of the time-scale variability of commonly used climate indices using continuous wavelet transform. Global and Planetary Change 78, 1-13.

Rueda, G., Fietz, S., Rosell-Mele, A., 2013. Coupling of air and sea surface temperatures in the eastern Fram Strait during the last 2000 years. Holocene 23, 692-698.

Rueda, G., Rosell-Melé, A., Escala, M., Gyllencreutz, R., Backman, J., 2009. Comparison of instrumental and GDGT-based estimates of sea surface and air temperatures from the Skagerrak. Organic Geochemistry 40, 287-291.

Sachse, D., Billault, I., Bowen, G.J., Chikaraishi, Y., Dawson, T.E., Feakins, S.J., Freeman, K.H., Magill, C.R., McInerney, F.A., van der Meer, M.T.J., Polissar, P., Robins, R.J., Sachs, J.P., Schmidt, H.-L., Sessions, A.L., White, J.W.C., West, J.B., Kahmen, A., 2012. Molecular Paleohydrology: Interpreting the Hydrogen-Isotopic Composition of Lipid Biomarkers from Photosynthesizing Organisms. Annual Review of Earth and Planetary Sciences 40, 221-249.

Schefuss, E., Ratmeyer, V., Stuut, J.-B.W., Jansen, J.H.F., Sinninghe Damsté, J.S., 2003. Carbon isotope analyses of n-alkanes in dust from the lower atmosphere over the central eastern Atlantic. Geochimica Et Cosmochimica Acta 67, 1757-1767.

Schefuss, E., Schouten, S., Schneider, R.R., 2005. Climatic controls on central African hydrology during the past 20,000 years. Nature 437, 1003-1006.

Schlesinger, M.E., Ramankutty, N., 1994. An oscillation in the global climate system of period 65-70 years. Nature 367, 723-726.

Schlitzer, R., 2010. Ocean Data View, http://odv.awi.de.

Schulz, M., Mudelsee, M., 2002. REDFIT: estimating red-noise spectra directly from unevenly spaced paleoclimatic time series. Computers & Geosciences 28, 421-426.

Shanahan, T.M., Hughen, K.A., Van Mooy, B.A.S., 2013. Temperature sensitivity of branched and isoprenoid GDGTs in Arctic lakes. Organic Geochemistry 64, 119-128.

Shindell, D.T., Schmidt, G.A., Mann, M.E., Rind, D., Waple, A., 2001. Solar Forcing of Regional Climate Change During the Maunder Minimum. Science 294, 2149-2152.

Sicre, M.A., Hall, I.R., Mignot, J., Khodri, M., Ezat, U., Truong, M.X., Eiríksson, J., Knudsen, K.L., 2011. Sea surface temperature variability in the subpolar Atlantic over the last two millennia. Paleoceanography 26, PA4218.

Sicre, M.A., Jacob, J., Ezat, U., Rousse, S., Kissel, C., Yiou, P., Eiriksson, J., Knudsen, K.L., Jansen, E., Turon, J.L., 2008a. Decadal variability of sea surface temperatures off North Iceland over the last 2000 years. Earth and Planetary Science Letters 268, 137-142.

Sicre, M.A., Yiou, P., Eiriksson, J., Ezat, U., Guimbaut, E., Dahhaoui, I., Knudsen, K.L., Jansen, E., Turon, J.L., 2008b. A 4500-year reconstruction of sea surface temperature variability at decadal time-scales off North Iceland. Quaternary Science Reviews 27, 2041-2047.

Siddall, M., Abe-Ouchi, A., Andersen, M., Antonioli, F., Bamber, J., Bard, E., Clark, J., Clark, P., Deschamps, P., Dutton, A., Elliot, M., Gallup, C., Gomez, N., Gregory, J., Huybers, P., Kawarnura, K., Kelly, M., Lambeck, K., Lowell, T., Milrovica, J., Otto-Bliesner, B., Richards, D., Stanford, J., Stirling, C., Stocker, T., Thomas, A., Thompson, B., Toernqvist, T., Vazquez Riveiros, N., Waelbroeck, C., Yokoyama, Y., Yu, S., Grp, P.L.W., 2010. The sea-level conundrum: case studies from palaeo-archives. Journal of Quaternary Science 25, 19-25.

Sikes, E.L., Volkman, J.K., Robertson, L.G., Pichon, J.-J., 1997. Alkenones and alkenes in surface waters and sediments of the Southern Ocean: Implications for paleotemperature estimation in polar regions. Geochimica Et Cosmochimica Acta 61, 1495-1505.

Sinninghe Damsté, J.S., Rijpstra, W.I.C., Hopmans, E.C., Weijers, J.W.H., Foesel, B.U., Overmann, J., Dedysh, S.N., 2011. 13,16-Dimethyl Octacosanedioic Acid (iso-Diabolic Acid), a Common Membrane-Spanning Lipid of Acidobacteria Subdivisions 1 and 3. Applied and Environmental Microbiology 77, 4147-4154.

Smittenberg, R.H., Eglinton, T.I., Schouten, S., Sinninghe Damsté, J.S., 2006. Ongoing Buildup of Refractory Organic Carbon in Boreal Soils During the Holocene. Science 314, 1283-1286.

Solanki, S.K., Usoskin, I.G., Kromer, B., Schussler, M., Beer, J., 2004. Unusual activity of the Sun during recent decades compared to the previous 11,000 years. Nature 431, 1084-1087.

Ternois, Y., Sicre, M.A., Boireau, A., Beaufort, L., Miquel, J.C., Jeandel, C., 1998. Hydrocarbons, sterols and alkenones in sinking particles in the Indian Ocean sector of the Southern Ocean. Organic Geochemistry 28, 489-501.

Trouet, V., Esper, J., Graham, N.E., Baker, A., Scourse, J.D., Frank, D.C., 2009. Persistent Positive North Atlantic Oscillation Mode Dominated the Medieval Climate Anomaly. Science 324, 78-80.

Vage, K., Pickart, R.S., Spall, M.A., Valdimarsson, H., Jonsson, S., Torres, D.J., Osterhus, S., Eldevik, T., 2011. Significant role of the North Icelandic Jet in the formation of Denmark Strait overflow water. Nature Geoscience 4, 723-727.

Vogts, A., Moossen, H., Rommerskirchen, F., Rullkotter, J., 2009. Distribution patterns and stable carbon isotopic composition of alkanes and alkan-1-ols from plant waxes of African rain forest and savanna C3 species. Organic Geochemistry 40, 1037-1054.

Vogts, A., Schefuss, E., Badewien, T., Rullkötter, J., 2012. n-Alkane parameters from a deep sea sediment transect off southwest Africa reflect continental vegetation and climate conditions. Organic Geochemistry 47, 109-119.

Waelbroeck, C., Labeyrie, L., Michel, E., Duplessy, J.C., McManus, J.F., Lambeck, K., Balbon, E., Labracherie, M., 2002. Sea-level and deep water temperature changes derived from benthic foraminifera isotopic records. Quaternary Science Reviews 21, 295-305.

Wang, G., Dolman, A.J., Alessandri, A., 2011. A summer climate regime over Europe modulated by the North Atlantic Oscillation. Hydrology and Earth System Sciences 15, 57-64.

Wanner, H., Solomina, O., Grosjean, M., Ritz, S.P., Jetel, M., 2011. Structure and origin of Holocene cold events. Quaternary Science Reviews 30, 3109-3123.

Wastl, M., Stötter, J., Caseldine, C., 2001. Reconstruction of Holocene Variations of the Upper Limit of Tree or Shrub Birch Growth in Northern Iceland Based on Evidence from Vesturardalur-Skidadalur, Trölaskagi. Arctic, Antarctic, and Alpine Research 33, 191-203.

Weijers, J.W.H., Bernhardt, B., Peterse, F., Werne, J.P., Dungait, J.A.J., Schouten, S., Sinninghe Damsté, J.S., 2011. Absence of seasonal patterns in MBT-CBT indices in mid-latitude soils. Geochimica Et Cosmochimica Acta 75, 3179-3190.

Weijers, J.W.H., Schefuss, E., Schouten, S., Sinninghe Damsté, J.S., 2007a. Coupled thermal and hydrological evolution of tropical Africa over the last deglaciation. Science 315, 1701-1704.

Weijers, J.W.H., Schouten, S., van den Donker, J.C., Hopmans, E.C., Sinninghe Damsté, J.S., 2007b. Environmental controls on bacterial tetraether membrane lipid distribution in soils. Geochimica Et Cosmochimica Acta 71, 703-713.

Zhu, C., Weijers, J.W.H., Wagner, T., Pan, J.-M., Chen, J.-F., Pancost, R.D., 2011. Sources and distributions of tetraether lipids in surface sediments across a large river-dominated continental margin. Organic Geochemistry 42, 376-386.

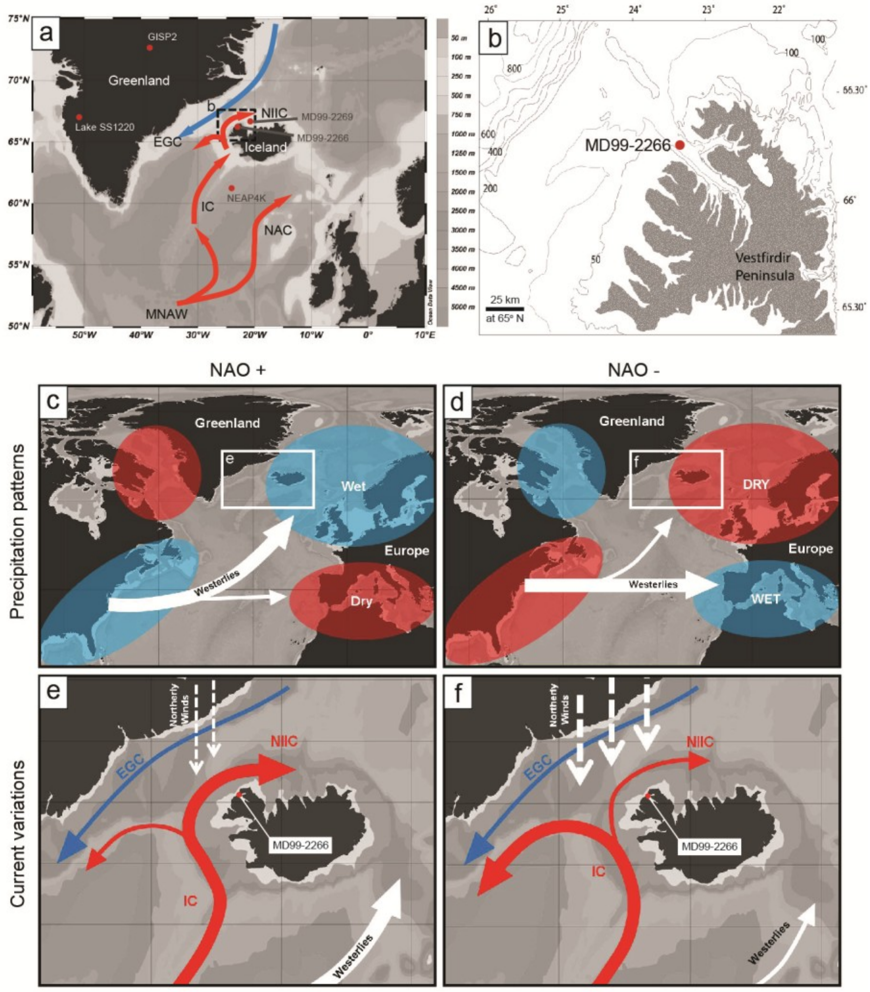

Figure 1: North Atlantic atmospheric and oceanic currents affecting the core (MD99-2266) location in the Denmark Strait. (a) Surface currents after Hansen and Østerhus (2000). Red arrows represent the Mean North Atlantic Water (MNAW) that branches into the North Atlantic Current (NAC) and the Irminger Current (IC). Part of the IC flows into the Denmark Strait and forms the North Icelandic Irminger Current (NIIC). The blue arrow represents the East Greenland Current (EGC). Core locations of compared datasets (Fig. 6), and of MD99-2266 are indicated by red dots. (b) Bathymetric map of Vestfirdir Peninsula with the core location (red dot) indicated in the mouth of Ísafjarðardjúp fjord. (c-f) Present day NAO influenced precipitation and current patterns. Iceland receives more precipitation during NAO+ (c), and less precipitation during NAO- (d) phases (Hurrell, 1995; precipitation patterns after: http://www.ldeo.columbia.edu/res/pi/NAO; Hurrell et al., 2003). NAO+ phases coincide with an increased Atlantic water influence on the North Icelandic Shelf and in the Denmark Strait, and decreased prevalence of northerly winds (e), and NAO- phases coincide with less Atlantic water influence in the Denmark Strait, and increased prevalence of northerly winds (f; Blindheim and Malmberg, 2005). Source of map:(Schlitzer, 2010).

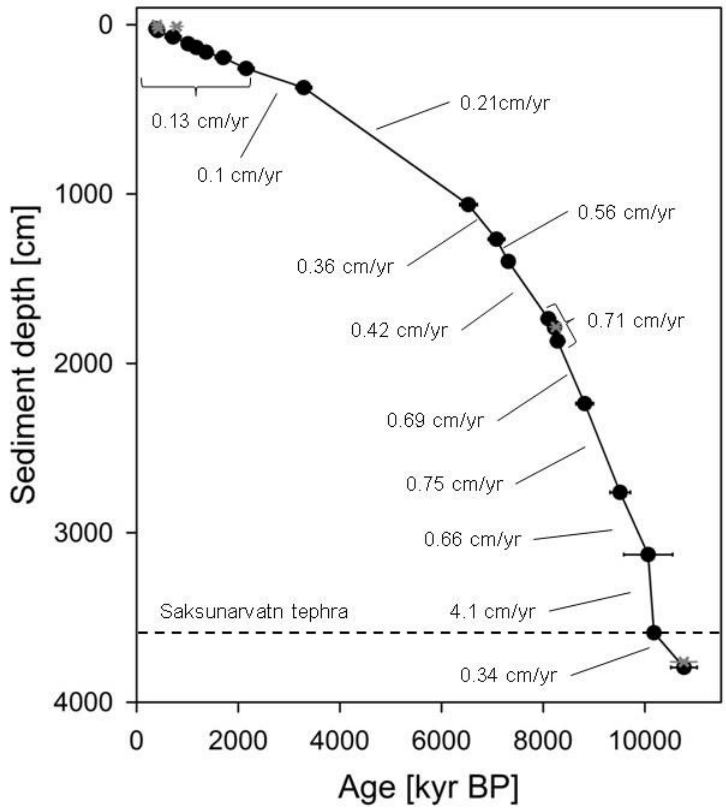

Figure 2: Age model of core MD99-2266 based on 19 (of a total of 24) ^{14}C-AMS dated sediment horizons and the depth horizon of the Saksunarvatn tephra (dashed line) which is dated at 10,180 ± 120 kyrs BP (Gronvold et al., 1995; Quillmann et al., 2010). The 5 ^{14}C-AMS dates discarded by Quillmann et al.(2010) are shown in grey. Sedimentation rates are calculated using the calibrated ages (kyr BP) of the dated horizons.

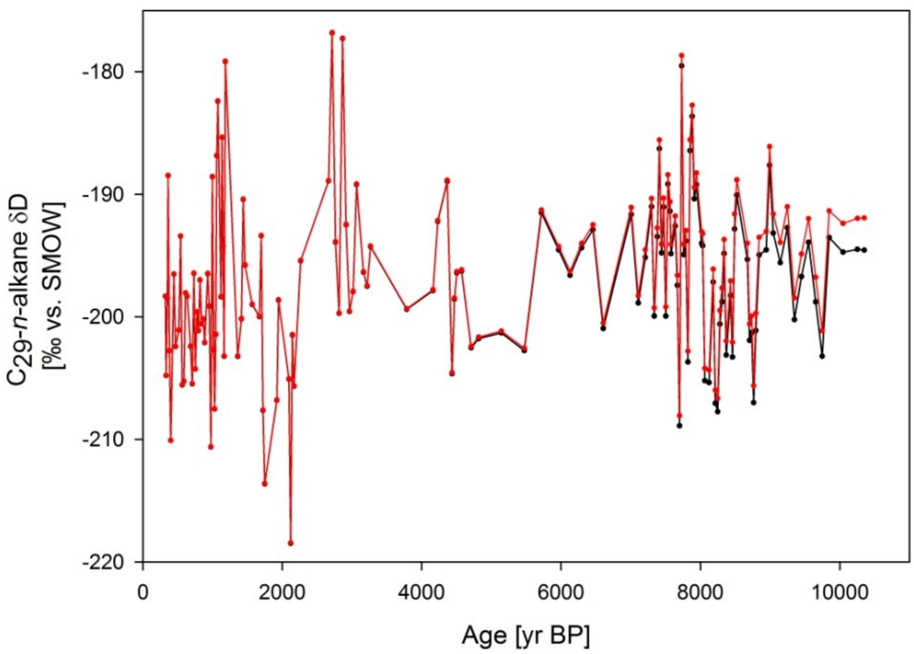

Figure 3: δD values of the C_{29}-*n*-alkane (black line and dots) and ice volume corrected δD values of the C_{29}-*n*-alkane (red line and dots).

1296

1297

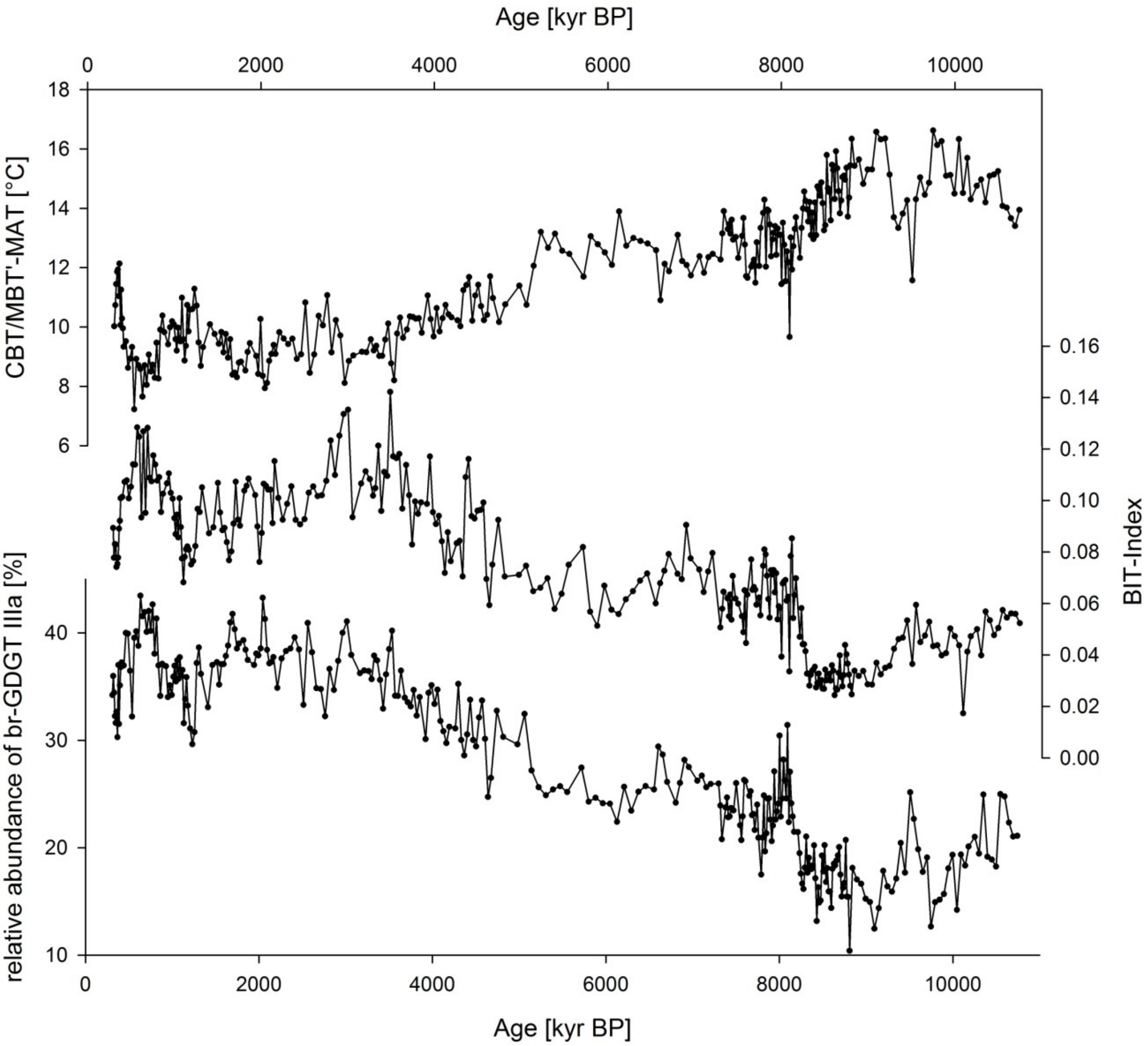

Figure 4: Temporal variability of the relative abundance of br-GDGT IIIa related to changes of the BIT-index (Moossen et al., 2013), and the CBT/MBT'-MAT reconstructions of Ísafjarðardjúp fjord.

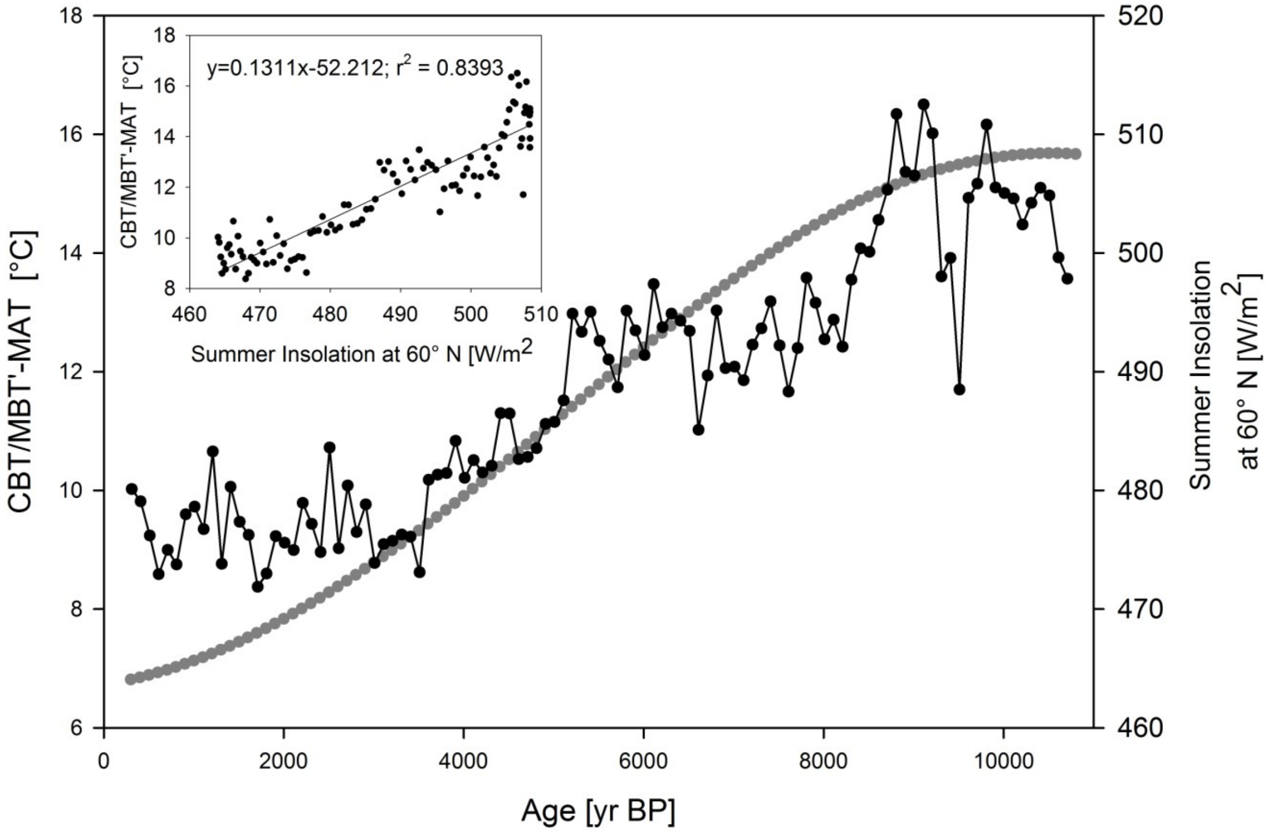

Figure 5: Regularly interpolated (sample interval = 100 years) CBT/MBT'-MATs (black dots and line) vs. summer insolation change (grey dots and line; sample interval = 100 years; Laskar et al., 2004). Inset: Linear correlation between CBT/MBT'-MAT and summer insolation.

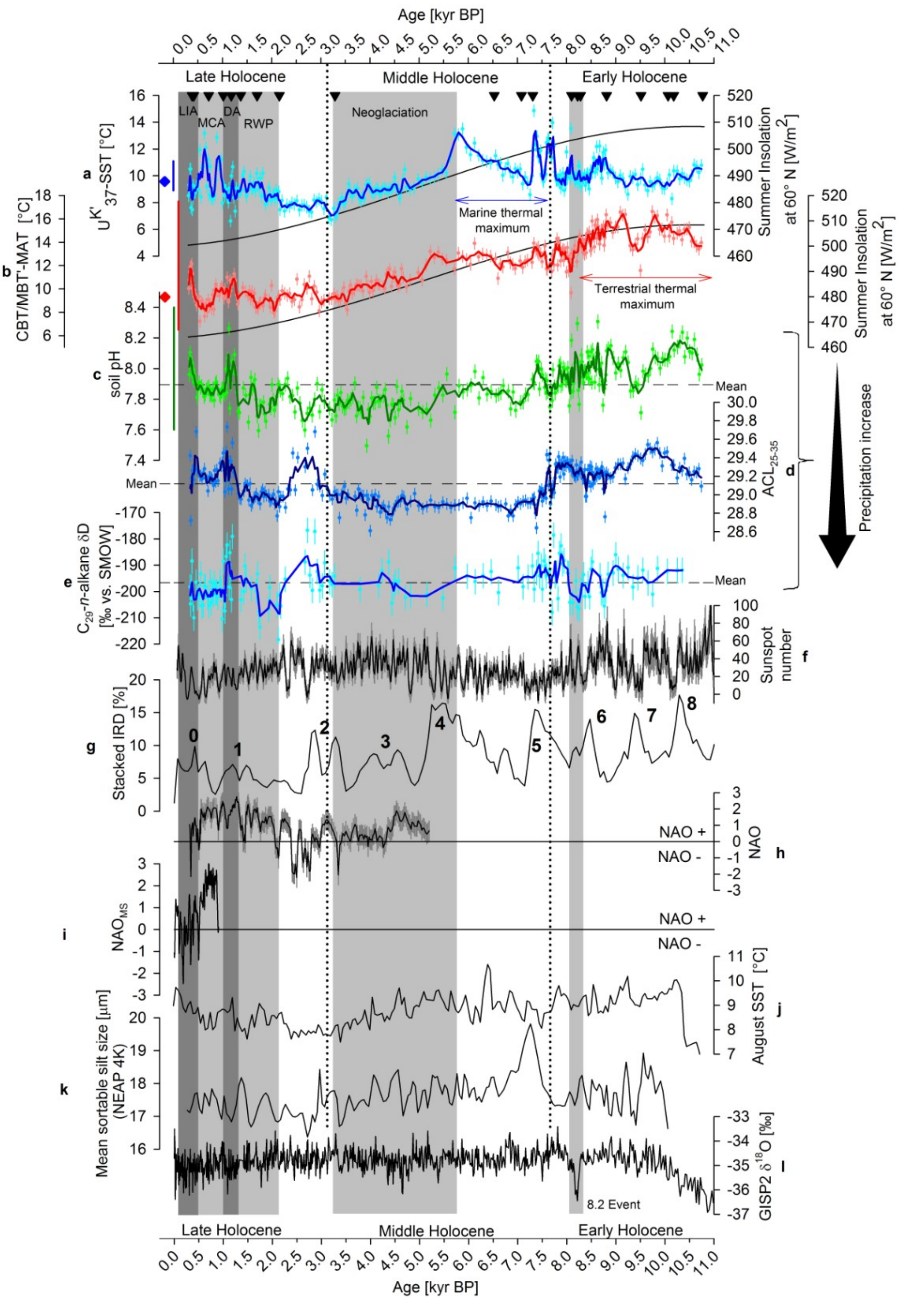

Figure 6: Iceland climate records compared with other North Atlantic paleoclimatic records. The LIA, MCA, DA (Dark Ages), RWP (Roman Warm Period), neoglaciation, and the 8.2 ka event are highlighted in shades of grey. The dotted horizontal lines indicate the division from early to middle, and from middle to late Holocene at 7.8 and 3.2 kyrs BP. **(a)** alkenone derived $U^{K'}_{37}$-SSTs. Raw data and 1σ SD (light blue) overlain by the 3-point moving average (dark blue), plotted against summer

insolation change (black line). The vertical blue bar indicates the uncertainty of the calibration equation (1.1 °C; Conte et al., 2006), the blue diamond indicates mean instrumental JJA SSTs at Stykkishólmur (Hanna et al., 2006). Black triangles indicate the ^{14}C-AMS dated horizons of MD99-2266. **(b)** br-GDGT derived CBT/MBT'-MAT. Raw data and 1σ SD (light red) overlaid by the 3-point moving (dark red) is plotted against summer insolation (black line). The vertical red bar indicates the uncertainty of the calibration equation (5.0 °C; Peterse et al., 2012). The red diamond indicates mean instrumental JJA air temperatures at Stykkishólmur (Hanna et al., 2004). **(c)** br-GDGT derived soil pH reconstruction. Raw data and 1σ SD (light green) overlain by the 3-point moving average (dark green). The vertical green bar indicates the uncertainty of the calibration equation (Root mean square error: 0.8; Peterse et al., 2012). **(d)** Average chain length variability of leaf wax derived *n*-alkanes (ACL_{25-35}) reconstructing precipitation variability. Raw data and 1σ SD (blue) overlain by the 3-point moving average (dark blue). **(e)** δD_{C29} reconstructing precipitation change. Raw data and 1σ SD (cyan) overlain by the 3-point moving average (blue). The dashed horizontal lines (c-e) indicate the mean Holocene precipitation as indicated by the respective records. **(f)** Holocene sunspot record (Solanki et al., 2004). **(g)** Stacked ice rafted debris (IRD) record revealing numbered Bond-cycles (Bond et al., 2001). **(h)** NAO variability after Olsen et al. (2012). **(i)** NAO variability after Trouet et al. (2009). **(j)** August SSTs on the North Icelandic Shelf after Justwan et al. (2008). **(k)** Mean sortable silt size of the Iceland-Scotland-Overflow-Waters (ISOW) south of Iceland after Hall et al. (2004). **(l)** GISP 2 δ^{18}O inferred temperature variations of the North Atlantic area after Grootes and Stuiver (1997).

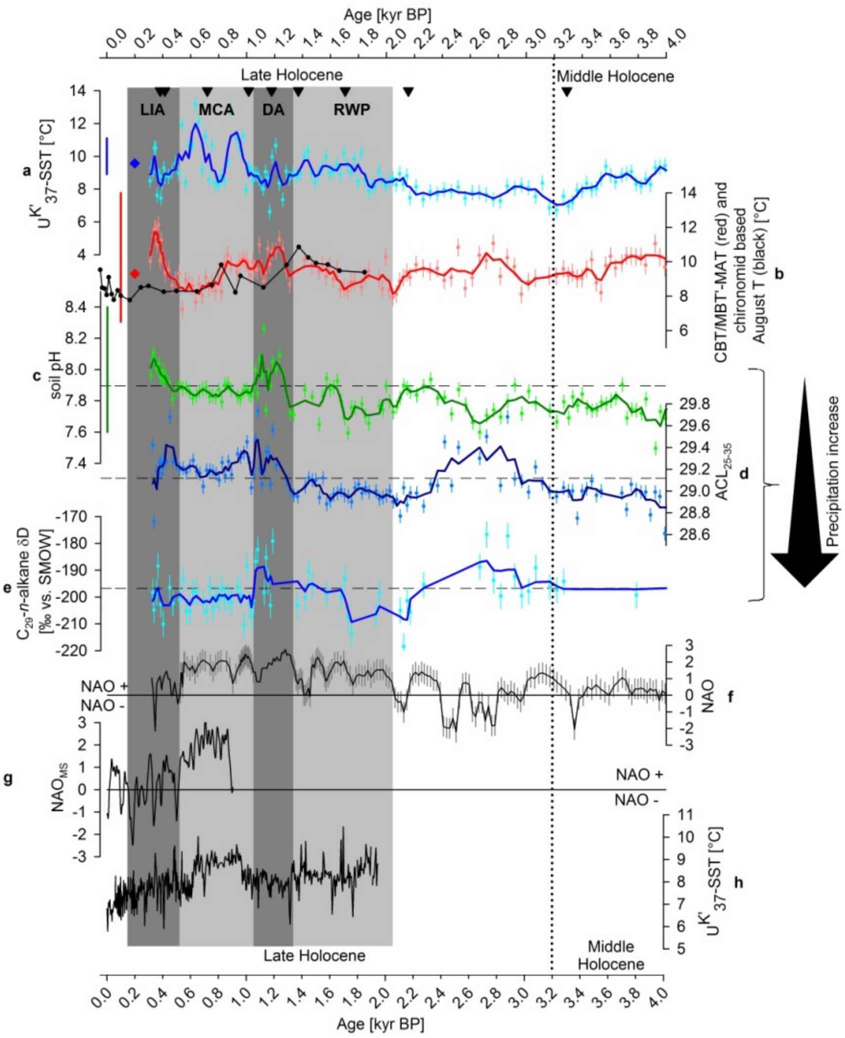

Figure 7: Iceland climate records of the youngest 4 kyrs BP. The LIA, the MCA, the DA, and the RWP are highlighted in shades of grey. The dotted horizontal line indicates the transition from the middle to the late Holocene. **(a)** $U^{K'}_{37}$-SST, raw data and analytical error (1σ SD) is shown in light blue overlain by the 3-point moving average in dark blue. The vertical blue bar indicates the uncertainty of the calibration equation (1.1 °C; Conte et al., 2006). The blue diamond indicates mean instrumental JJA SSTs at Stykkishólmur (Hanna et al., 2006). Black triangles indicate the ^{14}C-AMS dated horizons of MD99-2266. **(b)** CBT/MBT'-MAT raw data and analytical error (1σ SD) (light red) overlain by the 3-point moving average (dark red). The vertical red bar indicates the uncertainty of the calibration equation (5.0 °C; Peterse et al., 2012). The red diamond indicates mean instrumental JJA air temperatures at Stykkishólmur (Hanna et al., 2004). The black line and data points shows chironomide based August SSTs from north Iceland (Axford et al., 2009). **(c)** soil pH reconstruction raw data and analytical error (1σ SD; light green) overlain by 3-point moving average (dark green). The vertical green bar indicates the uncertainty of the calibration equation (0.8; Peterse et al., 2012). **(d)** Average chain length variability of leaf wax derived *n*-alkanes (ACL_{25-35}) raw data and analytical error (1σ SD; blue) overlain by the 3-point moving average (dark blue). **(e)** δD_{C29} raw data and analytical error (1σ SD; cyan) overlain by the 3-point moving average (blue). The dashed horizontal lines (c-e) indicate the mean Holocene precipitation as indicated by the respective records. **(f)** NAO variability after Olsen et al. (2012). **(g)** NAO variability after Trouet et al. (2009). **(h)** $U^{K'}_{37}$-SST reconstruction from the North Icelandic Shelf (Sicre et al., 2011).

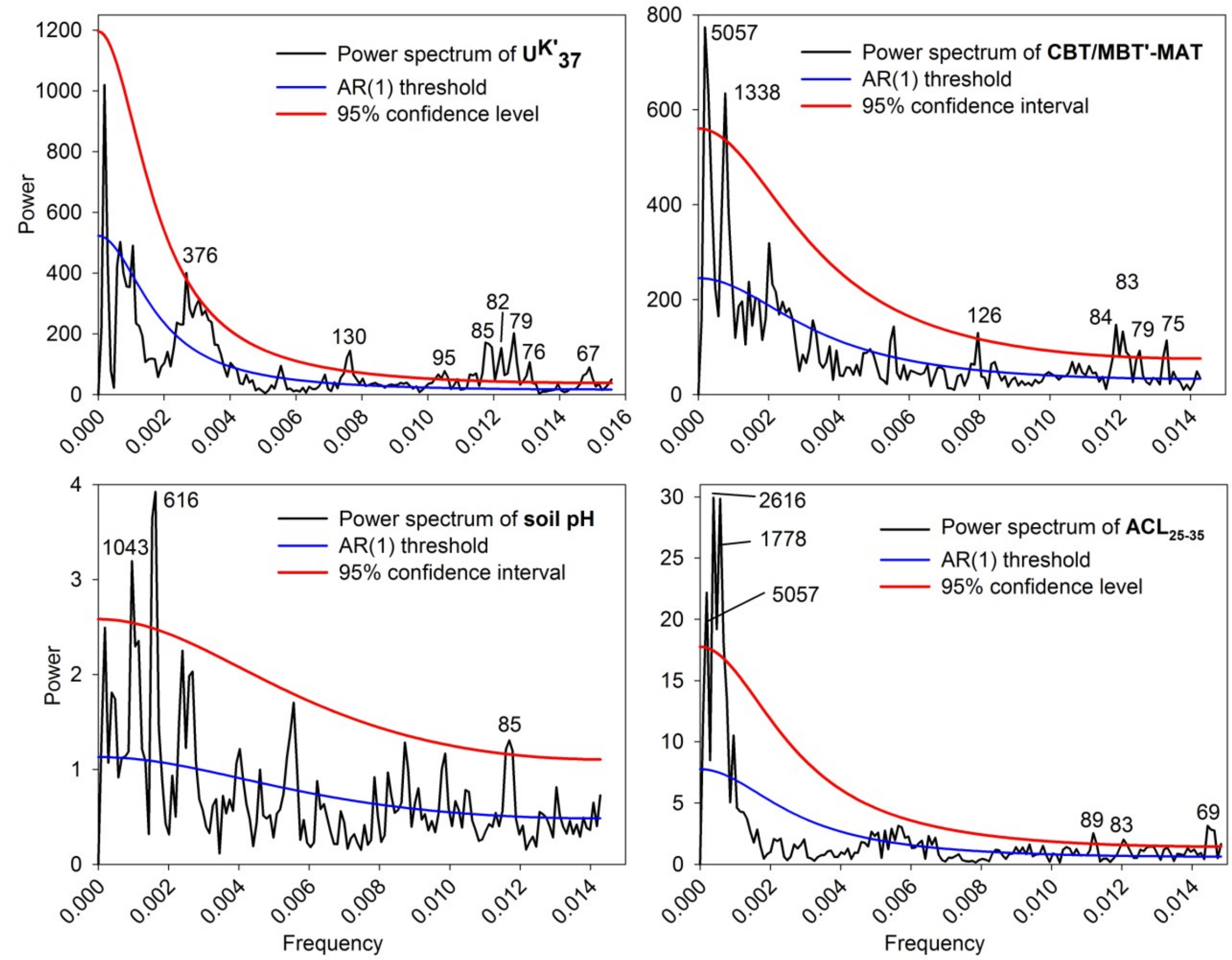

Figure 8: REDFIT power spectra of the $U^{K'}_{37}$-SST, CBT/MBT'-MAT, soil pH and ACL_{25-35} time series. The blue line delimits the AR(1) red noise model threshold. The red line indicates the 95 % confidence interval. The periodicities (years) of significant spectral peaks is indicated in each spectrum.